Systems/Circuits

GABAergic CaMKIIα+ Amygdala Output Attenuates Pain and Modulates Emotional-Motivational Behavior via Parabrachial Inhibition

Roni Hogri, Hannah Luise Teuchmann, Bernhard Heinke, Raphael Holzinger, Lidia Trofimova, and Jürgen Sandkühler

Department of Neurophysiology, Center for Brain Research, Medical University of Vienna, Vienna 1190, Austria

Pain and emotion are strongly regulated by neurons in the central nucleus of the amygdala (CeA), a major output of the limbic system; yet, the neuronal signaling pathways underlying this modulation are incompletely understood. Here, we characterized a subpopulation of CeA neurons that express the CaMKIIα gene (CeA^{CAM} neurons) and project to the lateral parabrachial nucleus (LPBN), a brainstem region known for its critical role in distributing nociceptive and other aversive signals throughout the brain. In male Sprague Dawley rats, we show that CeA^{CAM}-LPBN neurons are GABAergic and mostly express somatostatin. In anaesthetized rats, optogenetic stimulation of CeA^{CAM}-LPBN projections inhibited responses of LPBN neurons evoked by electrical activation of Aδ- and C-fiber primary afferents; this inhibition could be blocked by intra-LPBN application of the $GABA_A$ receptor antagonist bicuculline. CeA^{CAM}-LPBN stimulation also dampened LPBN responses to noxious mechanical, thermal, and chemical stimuli. In behaving rats, optogenetic stimulation of CeA^{CAM}-LPBN projections attenuated nocifensive responses to mechanical pressure and radiant heat, disrupted the ability of a noxious shock to drive aversive learning, reduced the defensive behaviors of thigmotaxis and freezing, induced place preference, and promoted food consumption in sated rats. Thus, we suggest that CeA^{CAM}-LPBN projections mediate a form of analgesia that is accompanied by a shift toward the positive-appetitive pole of the emotional-motivational continuum. Since the affective state of pain patients strongly influences their prognosis, we envision that recruitment of this pathway in a clinical setting could potentially promote pain resilience and recovery.

Key words: amygdala; analgesia; emotion; lateral parabrachial; motivation; pain

Significance Statement

Pain and emotion interact on multiple levels of the nervous system. Both positive and negative emotion may have analgesic effects. However, while the neuronal mechanisms underlying "stress-induced analgesia" have been the focus of many studies, the neuronal substrates underlying analgesia accompanied by appetitive emotional-motivational states have received far less attention. The current study focuses on a subpopulation of amygdala neurons that form inhibitory synapses within the brainstem lateral parabrachial nucleus (LPBN). We show that activation of these amygdalo-parabrachial projections inhibits pain processing, while also reducing behaviors related to negative affect and enhancing behaviors related to positive affect. We propose that recruitment of this pathway would benefit pain patients, many of whom suffer from psychological comorbidities such as anxiety and depression.

Received Oct. 8, 2021; revised Apr. 14, 2022; accepted Apr. 23, 2022.

Author contributions: R.Hog. and J.S. designed research; R.Hog., H.L.T., B.H., R.Hol., and L.T. performed research; R.Hog., H.L.T., B.H., R.Hol., and L.T. analyzed data; R.Hog. wrote the paper, with input from all other authors.

This work was supported by the Austrian Science Fund (FWF) Grant P29206-B27. We thank Claudia Klugmann for her excellent technical support during early stages of this project, Mariska Willemsen for her role in establishing parabrachial slice recordings, Todor Asenov and Thomas Adletzberger (IST workshop) for designing and manufacturing some of the equipment used in this study, and the Sandkühler laboratory for valuable discussions.

The authors declare no competing financial interests.

Correspondence should be addressed to Roni Hogri at roni.hogri@meduniwien.ac.at.

https://doi.org/10.1523/JNEUROSCI.2067-21.2022

Introduction

Pain is normally experienced as aversive, and as such enhances negative emotions and promotes defensive behavior while suppressing positive emotions and appetitive behavior (Rhudy and Meagher, 2001; Neugebauer et al., 2020). The effects of emotion on pain perception, on the other hand, seem to be more complex. For example, both positive and negative emotional states can potentially have analgesic effects (Rhudy and Meagher, 2001; Butler and Finn, 2009; Neugebauer et al., 2020). Yet, while positive emotion promotes healing and well-being, negative emotions promote defensive behaviors such as withdrawal and avoidance,

and over time may become maladaptive, leading to a worsening of existing pain conditions and the development of psychological comorbidities such as anxiety and depression (Karoly and Ruehlman, 2006; Lang and Bradley, 2010; Radat et al., 2013; Sturgeon et al., 2014).

Considered a major output of the limbic system, the central nucleus of the amygdala (CeA) integrates emotionally-relevant information and controls its downstream targets via GABAergic projections (Tovote et al., 2015; Neugebauer et al., 2020). Historically, data from studies involving indiscriminate experimental manipulations of CeA neurons (e.g., by electrical stimulation or lesions) have suggested that excitation of CeA neurons underlies the phenomenon of stress-induced analgesia, involving autonomic activation, aversion, and defensive behavior (Applegate et al., 1983; LeDoux et al., 1988; Helmstetter, 1992; Oliveira and Prado, 2001). Both CeA-evoked analgesia and defensive behaviors can be largely attributed to its projections to the periaqueductal gray (PAG), resulting in disinhibition of PAG projection neurons and indirect descending modulation of sensory and motor spinal circuits (LeDoux et al., 1988; Oliveira and Prado, 2001; Tovote et al., 2016).

Technological advancements over the past two decades have allowed for a more subtle dissection of amygdala circuitry and its connections to other brain regions. Genetically- and anatomically-defined subpopulations of CeA neurons have been described, with some seemingly encoding safety rather than danger, and driving appetitive rather than defensive behavior (Douglass et al., 2017; J. Kim et al., 2017). Intriguingly, it was recently shown that activation of a subpopulation of inhibitory neurons within the CeA had both analgesic and anti-aversive effects (Hua et al., 2020), an outcome that is inconsistent with activation of the canonical circuits involved in stress responses, and would arguably require a different form of descending modulation.

One potential target for CeA neurons modulating both pain perception and emotional-motivational state is the lateral parabrachial nucleus (LPBN). This brainstem nucleus is considered a key node in the ascending pain system, but also plays a critical role in emotional-motivational behavior (for review, see Gauriau and Bernard, 2002; Palmiter, 2018; Chiang et al., 2019). Specifically, excitation and disinhibition of LPBN neurons are associated with increased pain and defensive behaviors, while their inhibition results in pain attenuation and promotes appetitive behavior (Han et al., 2015; Rodriguez et al., 2017; Barik et al., 2018, 2021; Uddin et al., 2018; Chiang et al., 2020; Raver et al., 2020; Sun et al., 2020; Luskin et al., 2021). Previous reports have shown that the LPBN receives GABAergic inputs from the CeA, which are capable of inducing appetitive behavior and attenuating pain responses in rodents (Jia et al., 2005; Douglass et al., 2017; Raver et al., 2020).

Here, we report on the properties and functions of a population of LPBN-projecting CeA neurons. We show that most of these neurons express the calcium-calmodulin-dependent kinase IIα (CaMKIIα; CeA^{CAM}-LPBN neurons), as well as somatostatin. Selective optogenetic stimulation of CeA^{CAM}-LPBN projections resulted in inhibition of LPBN neurons both *in vitro* and *in vivo*, via $GABA_A$ receptor activation. In behaving rats, CeA^{CAM}-LPBN stimulation attenuated pain behavior, hindered the acquisition of aversive learning involving a noxious stimulus, reduced defensive behavior, and induced appetitive behavior. These results indicate that activation of this particular amygdalar output pathway induces analgesia as well as a shift toward a positive emotional-motivational state, potentially promoting recuperation.

Materials and Methods

Animals

All experiments were performed in male Sprague Dawley rats (40–100 g at the time of virus injection, marking the beginning of the experiment), bred in-house at the Medical University of Vienna, Austria. Throughout the experiment, rats were housed under standard laboratory conditions, with a 12/12 h light/dark cycle regime (light on at 6 A.M.) and *ad libitum* access to food and water. Experiments were performed during the light phase. All procedures were performed according to European Communities Council directives on the use of animals for scientific purposes (2010/63/EU), and were approved by the Ethics Committee for Advice and Assessment of Research Projects on Animals at the Medical University of Vienna, as well as the Austrian Federal Ministry of Education, Science and Research (BMBWF).

Virus injections

For retrograde tracing of CeA^{CAM}-LPBN neurons, herpes simplex viral vectors expressing mCherry under the control of either the ubiquitous cytomegalovirus (CMV) promoter (HSV1-CMV-mCherry), or of the CaMKIIα promoter (HSV1-CaMKIIα-mCherry; Viral Gene Transfer Core of the McGovern Institute for Brain Research at MIT) were injected unilaterally into the right LPBN. Adeno-associated viral vectors (AAVs) used in this study were obtained from the Neuroscience Gene Vector and Virus Core of Stanford University. For expression of channelrhodopsin-2 (ChR2) fused to the mCherry fluorophore under the control of the CaMKIIα promoter, $AAV_{2/DJ}$-CaMKIIα-hChR2 (H134R)-mCherry (AAV-ChR2) was injected into the CeA bilaterally, or unilaterally into the right CeA for some *in vivo* electrophysiology experiments (see below). Control rats received intra-CeA injections of $AAV_{2/DJ}$-CaMKIIα-mCherry (AAV-mCherry), which does not include the gene for ChR2. Rats were placed in an anesthesia induction chamber and received 5% isoflurane in 6–8 l/min O_2. After loss of consciousness, rats received a cocktail of ketamine and xylazine (50 and 2.5 mg/kg, i.p., respectively). Carprofen (4 mg/kg, s.c.) was administered for perioperative analgesia. The head was shaved and fixed in a stereotaxic frame, and the isoflurane anesthesia titrated (0.5–3% in 0.6–0.8 l/min O_2, delivered via a mask mounted on the mouthpiece of the stereotaxic frame) to achieve a stable state of deep anesthesia, determined by the absence of withdrawal reflexes to hindpaw pinch. Core body temperature was maintained at 37°C using a heating pad (Panlab). The scalp was incised, and a craniotomy performed to allow access to the LPBN (1.8 mm laterally and 0.5 mm caudally to the apex of the lambdoid suture) or CeA (3.8 mm laterally and 1.5–2 mm rostrally to the bregma). A microsyringe (Hamilton) was mounted onto a motorized stereotaxic microinjector (IMS-20, Narishige), and loaded with the appropriate viral vector. Injection procedures were adjusted for intra-LPBN and intra-CeA injections, to maximize vector delivery throughout the rostrocaudal plane of each target, while minimizing spill-over (see examples in Results). The microsyringe needle was slowly lowered toward the brain target, with the needle tip facing caudally at a 7- or 20-degree angle for LPBN and CeA injections, respectively. Injection depths (from the brain surface) were 6.2 mm for the LPBN and 7.5 mm for the CeA. The microsyringe was kept in place for 5 min before injection commenced. For intra-LPBN and intra-CeA injections, 0.4 and 1 µl of virus solution was infused, respectively, at a rate of 0.1 µl/min; once injection was completed, the microsyringe was left in place for an additional 5–10 min before being slowly retracted. Following virus injections, rats were allowed a period of gene expression before additional procedures took place. Experiments in acute brainstem slices (see below) revealed robust expression of ChR2-mCherry in CeA axons at the LPBN level as early as four weeks after AAV injection. Nevertheless, *in vivo* optogenetic experiments were performed in adult rats (at least three months old), at least eight weeks after virus injection. For experiments involving HSV1-based retrograde labeling of CeA^{CAM}-LPBN neurons, brains were removed six weeks after virus injection.

In vitro whole-cell patch-clamp recordings

Brain slice preparation

Rats were deeply anaesthetized with isoflurane (5% in O_2) and decapitated. The brain was quickly removed and kept in preoxygenated (95% O_2 and 5% CO_2) ice-cold incubation solution, which consisted of (all in mM): 95 NaCl, 1.8 KCl, 1.2 KH_2PO_4, 0.5 $CaCl_2$, 7 $MgSO_4$, 26 $NaHCO_3$, 15 glucose, and 50 sucrose, pH 7.4; osmolarity = 310–320 mOsm/l. A vibrating microslicer (DTK-1000, Dosaka) was used to prepare 350-μm-thick coronal brain slices containing the LPBN. Brain slices were kept in oxygenated incubation solution at 33–34°C for 30 min, and then at room temperature until further use.

In vitro *electrophysiological recordings*

Brain slices were transferred into a recording chamber and constantly super-fused (rate = 3–4 ml/min; IP High Precision Multichannel Pump, Ismatec) with oxygenated recording solution, which consisted of (all in mM): 127 NaCl, 1.8 KCl, 1.2 KH_2PO_4, 2.4 $CaCl_2$, 1.3 $MgSO_4$, 26 $NaHCO_3$, and 15 glucose, pH 7.4; osmolarity = 310–320 mOsm/l. The LPBN was localized using a x4 objective on an upright microscope (Olympus BX51WI, Olympus Optical) connected to a camera (PCO) and Dodt infrared optics (Luigs & Neumann) via visual landmarks, mainly the superior cerebellar peduncle. For the whole-cell patch-clamp approach, LPBN neurons were visualized with a 40× 0.8 N.A. water immersion objective. A horizontal micropipette puller (Model P-1000, Sutter Instrument) was used to prepare patch pipettes (2–4 MΩ) from borosilicate glass tubes (GB200F-8P, Science Products). Patch pipettes were filled with intracellular solution, consisting of (all in mM): 120 potassium gluconate, 20 KCl, 2 $MgCl_2$, 20 HEPES, 0.5 Na-GTP, 0.5 Na_4-EGTA, and 2 Na_2-ATP, pH 7.28 (adjusted with KOH), osmolarity = 280–300 mOsm/l.

Recordings were performed in voltage-clamp mode with a holding potential of −70 mV, using a patch-clamp amplifier (Axopatch 200B), a digitiser (Digidata 1440A) and pCLAMP 10 acquisition software (all from Molecular Devices). Under these recording conditions, the equilibrium potential for both Na^+ and Cl^- was more positive than the holding potential, resulting in inward currents for both ions. Only cells with a resting membrane potential equal or more negative than −45 mV and with a series resistance below 25 MΩ were used for experiments. CeA^{CAM} axons in the LPBN were activated by 10-ms pulses of blue light (470 nm), delivered by an optical fiber (1-mm diameter, 0.48 N.A., Thorlabs) and produced by a driver-powered light-emitting diode (LEDD1B, Thorlabs). Only neurons in which photostimulation induced postsynaptic currents (PSCs) that could follow a 10 × 10 Hz stimulation with a failure rate of ≤10% were used for further analyses. Light-evoked PSCs were recorded for at least 15 min, with a light pulse given every 30 s. To monitor the series resistance, a voltage step to −80 mV was applied 100 ms before each light pulse; only experiments with a maximum variance of ±25% of the series resistance were included in further analyses. Signals were low-pass filtered (2–10 kHz) and sampled at 100 kHz. Analysis was performed offline using Clampfit 10.7 Software (Molecular Devices). We did not correct for the liquid junction potential.

Drugs and drug application

All drugs were prepared in stock solutions and diluted in 20-ml recording solution to reach the desired concentration, and applied in a closed system via super-fusion of the recording chamber. The following drugs were added during electrophysiological recordings (solvent of stock solutions is given as well): the AMPA/kainate receptor antagonist CNQX (10 μM, dimethyl sulfoxide, Abcam), and the $GABA_A$ receptor antagonist bicuculline (10 μM, deionized distilled H_2O, Sigma-Aldrich). Drugs were applied with an interapplication interval of 5 min.

In vivo extracellular recordings

Surgery

Rats were deeply anaesthetized using a ketamine/xylazine mixture (initial dose of 110 and 10 mg/kg, i.p., respectively). A tracheotomy was performed and animals were intubated with a 14G cannula, for mechanical respiration with a microventilator (10–30 mbar O_2, 75–90 pulses/min; UMV-03, Uno). The jugular vein was exposed and cannulated, and the head fixed into a stereotaxic frame. A craniotomy was performed over the right LPBN (or over both LPBNs, for some experiments involving intra-LPBN microinjections, as described below), and the left sciatic nerve was exposed and connected to a bipolar hook stimulation electrode. A syringe mounted onto a motorized injector (AL-300, World Precision Instruments) and connected to the jugular cannula was used for continuous IV delivery (4 ml/kg/h) of a solution consisting of: Ringer's solution (54.5%), 6% hydroxyethyl starch 130/0.4 in 0.9% NaCl (26%), glucose (7%), 10% ketamine hydrochloride, and 2% xylazine hydrochloride (5% and 2.5%, respectively) for anesthesia maintenance, and 0.2% pancuronium bromide (5%) for muscle relaxation. A vital sign sensor (MouseOX Plus, STARR Life Sciences Corp.) was attached to the right hindpaw of the rat, and allowed for online monitoring of blood oxygen saturation, pulse distention and pulse rate throughout the experiment.

Recording configuration

An "optetrode" (Thomas Recording GmbH), consisting of a single-shaft platinum/tungsten tetrode (0.5–0.8 MΩ; O.D. = 100 μm) connected to an optic fiber (O.D. = 120 μm, 0.66 N.A., tip positioned 250 μm above tetrode tip), was inserted into the brain 2–2.5 mm laterally and 1.5–2.5 mm rostrally to the λ, with the optic fiber positioned rostrolaterally to the tetrode. The optetrode was advanced toward the LPBN at a 7° angle (tip facing caudally), under electrophysiological control (average recording depth = 5.6 mm from the brain surface). To allow for post-mortem identification of recording locations, optetrode tips were shortly dipped in a solution containing the fluorescent dye 1,1'-dioctadecyl-3,3,3',3'-tetramethylindodicarbocyanine, 4-chlorobenzenesulfonate salt (DiD; 5% w/v in 2:1 acetone:methanol) before insertion. In some rats, recordings were performed from 2 electrophysiologically distinct locations within the LPBN; the minimal distance between two recording sites in the same rat was 190 μm. Extracellular activity was digitized at 30 kHz per channel (HS-16-MUX and Digital Lynx 4SX, Neuralynx), and band-passed online (0.5–3 kHz; Cheetah 5, Neuralynx) to record action potentials. For optogenetic stimulation, a train (10-ms pulses at 20 Hz; 2100 isolated pulse stimulator, AM Systems) of blue light (473-nm wavelength) was delivered from a laser source (OptoSolo, IkeCool) to the optetrode via a patch cord (105-μm core diameter, 0.22 N.A.); the light power was set to ∼15 mW as measured directly below the optetrode tip (S121C sensor and PM100D power meter console, Thorlabs).

Delivery of noxious stimuli and optogenetic stimulation

Neuronal LPBN responses to electrical sciatic nerve stimulation (0.5-ms pulses, 15-s interstimulus interval; Isostim ISO-01D-100, npi electronic GmbH) were recorded in experiments consisting of 40 weak stimuli (1 V) and 40 strong stimuli (15 V; order counterbalanced between experiments); these stimulation intensities were found to be consistently subthreshold and suprathreshold for the activation of C-fiber primary afferents, respectively (unpublished data). The sciatic nerve was stimulated in alternating laser off and laser on trials; in laser on trials, a 6-s blue light train was triggered 5 s before nerve stimulation. To examine LPBN neuronal responses to noxious mechanical pressure and radiant heat, calibrated forceps (Rodent Pincher, Bioseb) and infrared (IR) laser (980 nm; Photontec Berlin), respectively, were applied to the left hindpaw. In experiments involving noxious pinch, the minimal force for eliciting firing in at least one recorded neuron was determined in real time. Then, 40 pinches (1 s in duration, 30-s interstimulus interval) of varying suprathreshold intensities were applied in alternating "laser off" (control) and "laser on" trials; the experimenter was blind to the neuronal activity during testing. In laser on trials, a 6-s blue laser train was triggered 5 s before the application of the pinch. In radiant heat experiments, IR light was delivered through a patch cord (200-μm core diameter, 0.22 N.A.), the end of which was positioned ∼15 mm from the hindpaw. Once a receptive field was identified, 20 IR stimuli (5-s pulses, 30-s interstimulus interval) were applied in alternating laser off and laser on trials. In laser on trials, an 11-s blue laser train was triggered 5 s before IR onset. Capsaicin (1%, 0.1 ml, intraplantar; Tocris Bioscience) was injected into receptive fields of neurons responding to either pinch or

radiant heat. LPBN activity was recorded for 15 min, starting 5 min before capsaicin injection; 15-s blue laser trains (laser on blocks) were separated by 15-s periods without laser stimulation (laser off blocks) throughout. The timing of capsaicin injection (during a laser off or laser on block) was counterbalanced between experiments. When multiple experiments were performed in the same rat, experiments involving sciatic nerve stimulation or pinch always preceded radiant heat experiments, and capsaicin experiments were the last to be performed.

Intra-LPBN microinjections

In a separate cohort of rats, we examined the effects of intra-LPBN bicuculline on the ability of CeA^{CAM}-LPBN stimulation to inhibit LPBN responses to electrical stimulation of the sciatic nerve. For this, rats received intra-CeA injections of AAV-ChR2, either bilaterally or unilaterally (right CeA). Subsequently, an optetrode equipped with an injection cannula (O.D. 115 µm, tip positioned caudomedially and 250 µm ventrally to tetrode tip; Thomas Recording GmbH) was inserted into the right or left LPBN (ipsilateral to the injected CeA), and neuronal responses to weak and strong electrical stimulation of the left sciatic nerve in alternating laser off and laser on trials were recorded as described above. Once laser-induced inhibition was detected (minimum of 20% reduction in at least one response component and 10% reduction overall, see below), 250 nl of either bicuculline methiodide (4 mM) or vehicle (saline) were injected into the LPBN at a rate of 100 nl/min. Responses to sciatic nerve stimulation in laser off and laser on trials were repeated 15–45 min after microinjection. A maximum of one experiment per hemisphere (and two recording locations per rat) was performed.

Analysis of in vivo *electrophysiological data*

All data collected in *in vivo* electrophysiology experiments were analyzed offline in Spike2 (Cambridge Electronic Design Ltd.), using bespoke programs written in the Spike2 language. In sciatic nerve stimulation experiments, the electrical stimulus evoked synchronous firing of multiple units in close succession, which precluded reliable spike sorting in the majority of cases; therefore, data were treated as a multiunit activity (MUA) signal. Spiking events were extracted by thresholding the MUA signal. Waveforms were first rectified, and waveforms crossing the threshold level, calculated as mean + 7 × SD of baseline, were further examined; only waveforms whose nonrectified peak-to-peak amplitude was at least twice the threshold value were marked as spiking events and were included in subsequent analyses. The minimal interspike interval was set to 1.5 ms. For both the weak (1 V) and strong (15 V) nerve stimulation intensities, strong phasic population activity was observed in the range of 7–80 ms poststimulus (early response component); we attribute this early response component to spinoparabrachial inputs driven by the activation of A-type primary afferents (mostly Aδ-fibers). In strong nerve stimulation trials, an additional late response component was observed in the range of 80–1000 ms (but usually terminating within the first 250 ms postnerve stimulation). Analysis of laser effects was restricted to time bins in which a response to nerve stimulation occurred. Bin duration was set to 10 ms (sliding window, 5-ms steps) for the early component, and 30 ms (10-ms steps) for the late component. For both components, the response threshold was set to the mean + 5 × SD of the firing rate during baseline periods (10–5 s before the nerve stimulation, to exclude the time of optogenetic stimulation), in addition, to be considered suprathreshold, firing had to be detected within a given bin in >20% of trials.

For experiments involving pinch, radiant heat, and capsaicin, spikes were sorted based on their relative contribution to the waveforms of the four recording channels. For this, spikes from each channel were first thresholded based on peak-to-peak amplitude; suprathreshold spikes were sorted based on template matching and principal component analysis, taking into account all recorded channels. Next, it was determined whether each extracted unit responded to the noxious stimulus in question. For pinch and radiant heat stimuli, the firing rate during the baseline period (10–5 s before the onset of noxious stimuli) was compared with the firing rate in predefined periods after the onset of the noxious stimulus (0–3 s for pinch and 3–8 s for radiant heat). Within these predefined periods, 1-s bins (sliding window, 0.5-s steps) were examined to determine whether the firing rate within each time bin was higher than the mean + 2 × SD of baseline. In addition, since most LPBN neurons exhibited low spontaneous firing, to qualify as a response bin, firing had to be detected within a given suprathreshold bin in >40% of trials. For capsaicin experiments, a unit was considered responsive if it showed a significantly elevated firing rate compared with baseline (one-sided Wilcoxon matched-pairs signed rank test, $p < 0.05$) during at least five consecutive min in the period of 30–600 s following the injection; for this analysis, only laser off blocks were considered. The effect of photostimulation on capsaicin-evoked activity was tested for the period of 30–600 s postinjection; the first 30 s following injection were excluded from analysis to minimize the contribution of mechanical stimulation to the analyzed activity. To avoid contamination of the data by delayed effects of laser onset and offset, only the last 10 s of laser off and laser on blocks were included in these analyses.

Behavioral experiments

Optic fiber implantation

Rats were anaesthetized with a combination of a ketamine/xylazine injection (50 and 5 mg/kg, i.p., respectively) and isoflurane (1–3% in 1 l/min O_2) delivered through a mask mounted on the mouthpiece of the stereotaxic frame (Narishige). Carprofen (4 mg/kg, s.c.) was administered for perioperative analgesia, the head was fixed using nonrupturing ear bars, the scalp was incised and retracted, and the surface of the skull cleaned. Craniotomies were performed over the LPBN bilaterally and four surgical screws (1.2 mm in diameter; Precision Technology Supplies Ltd.) were inserted into the skull for implant fixation. Optic fibers (core diameter 200 µm, 0.22 N.A.) fitted into ceramic ferules were slowly advanced into the brain at a 7° angle, such that their tips were positioned above the LPBN (insertion location 2.2 mm laterally and 2.2 mm rostrally to the λ, depth of 5.2 mm from brain surface). Optic fibers were fixed in place using a combination of UV light-sensitive cement (Tetric EvoFlow, Ivoclar Vivadent) and bone cement (Refobacin, Biomet). Rats were allowed at least one week of recovery before behavioral procedures began.

General experimental procedures

All behavioral experiments were conducted on intermingled groups of rats injected with AAV-ChR2 or the control vector AAV-mCherry. The experimenter was blind to group allocation of each rat during testing and data extraction. When applicable, lab equipment was triggered using an I/O card (USB-6002, NI), controlled by bespoke MatLab scripts (MathWorks Inc.). Laser stimulation (473-nm wavelength) was delivered to the implanted optic fibers through patch cords (200 µm, 0.22 N.A.) connected to the laser source (OptoSolo) via a beam splitter/rotary joint (Doric Lenses), in trains of 10-ms pulses, at a frequency of 20 Hz. In experiments involving tracking or analysis of freezing, sessions were video recorded with a USB camera (DFK 22BUC03, The Imaging Source GmbH), controlled by Viewer3 (Biobserve).

Nocifensive responses to mechanical and thermal stimulation

Mechanical and heat sensitivity were measured using the von Frey and Hargreaves tests, respectively, in separate cohorts of animals. Rats were habituated to the experimenter and experimental apparatus on two consecutive days. Baseline paw withdrawal measurements were performed on 2 d. On the third day of testing (day 0), rats were shortly anaesthetized with isoflurane (5% in 6 l/min O_2 for 1 min), and 1% capsaicin (0.1 ml, intraplantar; Tocris Bioscience) was injected into left hindpaw; an additional paw withdrawal measurement commenced 30 min thereafter. In both types of threshold tests, paws were stimulated in alternating laser off and laser on trials; the minimal interval between measurements was 5 min. In all sessions, paws were stimulated either in the absence or presence of optogenetic stimulation of CeA^{CAM}-LPBN axons (laser off and laser on conditions, respectively); conditions were alternated between each two measurements from the same paw. In laser on trials, a 30-s laser train was triggered by the experimenter 5–10 s before the onset of paw stimulation. Paw withdrawal responses were scored separately for each paw in each condition (laser off/on). For the von Frey test, the 50% paw withdrawal threshold was

assessed using the simplified up-down method, as previously described (Bonin et al., 2014; Hadschieff et al., 2020). Briefly, each paw was stimulated five times per condition. For each stimulation, von Frey filaments were applied to the plantar surface of the hindpaw for up to 5 s, or until paw withdrawal. If the paw was withdrawn, a lighter filament was used for the next stimulation of the same paw in the same condition; otherwise, a higher force filament was used. For the Hargreaves test, the paw withdrawal latency to radiant heat was calculated as previously described (Hargreaves et al., 1988; Xanthos et al., 2011). Briefly, rats were placed on a glass floor, and an IR lamp (Stoelting) was used to generate a radiant beam aimed at the plantar surface. The intensity of the IR beam was adjusted to elicit a mean withdrawal latency of ~12 s in laser off trials of the first baseline session. In each trial, radiant heat was applied until paw withdrawal, or until the 20-s cutoff was reached. For each session, the withdrawal latency for each hindpaw was calculated as the average of two measurements performed per condition.

Unconditioned responses and aversive learning induced by noxious shocks

To examine how CeA^{CAM}-LPBN stimulation would affect both innate and learnt responses to a noxious input, rats underwent a single fear conditioning session (day 1). The conditioning chamber (L × W × H = 80 × 38 × 40 cm; Institute of Science and Technology; IST), was equipped with a grid floor for foot-shock delivery (cleaned with 70% ethanol), and a wall-mounted loudspeaker; the walls were covered with visual markings. Rats were placed in the conditioning chamber and allowed to explore freely for 2 min before conditioning began. Then, rats received two pairings of a tone conditioned stimulus (tone-CS; 10 s, 2 kHz, 70 dB; AFG-2225, GW-Instek) and a co-terminating electrical shock (1 mA, 0.5 s) generated by a shocker/scrambler (LE100-26, Panlab) as the unconditioned stimulus (shock-US (unconditioned stimulus)), with an intertrial interval of 5 min; pilot experiments showed that this conditioning procedure resulted in robust conditioned freezing to the tone-CS (conditioned stimulus). In each trial, laser stimulation was delivered for 2 s, beginning 1 s before the onset of the shock-US. On day 2, rats underwent a "cue test" session, in which they were placed in a test chamber (L × W × H = 80 × 44 × 40 cm; IST), that was distinct from the conditioning chamber in terms of floor (black Plexiglas), odor (5% acetic acid), and visual patterns on the surrounding walls. After 2 min of habituation to the test chamber, the tone-CS was delivered for three consecutive minutes. Freezing behavior during the first 2 min after each shock in the conditioning session, as well as during tone-CS presentation in the cue test session, was manually scored offline by a trained experimenter. In order to be considered a freezing bout, the rat had to stay completely still (except for respiration-related movement) for a minimum of two consecutive seconds.

Defensive behaviors

The effect of laser stimulation on defensive behavior was tested using two paradigms: thigmotaxis in an open field arena, and freezing (Barnett, 1963; Sullivan et al., 2003; Fanselow et al., 2019; Mobbs et al., 2020). Thigmotaxis behavior was assessed in a subset of rats previously tested for heat sensitivity, 3 d following the last session of threshold testing. Rats were placed in an open field arena (L × W × H = 80 × 95 × 40 cm; IST) for 10 min, and laser stimulation was delivered throughout. To quantify thigmotaxis behavior, the location of rats was automatically tracked (Viewer3) and the thigmotaxis score was calculated as the % of time in which the body center was within 15 cm of the walls. To assess the effect of laser stimulation on freezing, a separate cohort of rats were first fear conditioned as described above. The conditioning session (day 1) consisted of three pairings of tone-CS and shock-US (2 mA, 0.5 s), delivered with 2-min intertrial intervals; pilot experiments showed this conditioning procedure induced robust conditioned freezing to both the context (conditioning chamber) and the tone-CS. On day 2, rats underwent two test sessions, a context test and cue test, which were separated by 4 h. In the context test session, rats were placed in the conditioning chamber for 5 min, and laser stimulation was delivered for 2 min, 1–3 min after the test began. In the cue test session, rats were placed in a novel chamber; after 2 min of habituation, the tone-CS was delivered for 3 min, and laser stimulation was delivered for 2 min, 1–3 min after tone commencement. On day 5, a cue-retest session took place, which was identical to the cue test session, except that no laser stimulation was given. Scoring of freezing during all test sessions was performed as described above.

Appetitive behaviors

To evaluate the effect of CeA^{CAM}-LPBN stimulation on appetitive behaviors, we examined the ability of laser stimulation to induce real-time place preference (RTPP) and food consumption (Bardo and Bevins, 2000; Lang and Bradley, 2010; Douglass et al., 2017). The RTPP paradigm consisted of two daily sessions. On day 1 (baseline session), rats were placed in the center of a behavioral arena divided into two compartments (80 × 47 cm each), separated by a passageway (30 cm) that allowed for free passage between both compartments. The two compartments were distinct from each other in odor (30% ethanol and 1% acetic acid) and visual patterns on the walls. Rats were allowed to freely explore the arena for 10 min, while receiving no laser stimulation. On day 2, rats in the AAV-mCherry-Capsaicin and AAV-ChR2-Capsaicin groups received intraplantar capsaicin injections, as described above; rats in the AAV-ChR2-No Pain group were handled, but not injected; 30 min later, the test session took place. Rats were placed in the center of the arena, and allowed to explore freely. Once a rat entered the predesignated pseudorandomally-assigned "laser compartment", laser stimulation began, and was delivered whenever the rat occupied this compartment during the subsequent 10 min. To assess the degree to which rats experienced laser stimulation as rewarding, the % of time the rat spent in the laser compartment during the relevant 10-min period in the baseline and test sessions was compared. To examine the effect of laser stimulation on food consumption, sated rats were placed in a clear Plexiglas box (L × W × H = 21 × 21 × 28 cm) with normal chow pellets. Following 30 min of habituation, laser stimulation was delivered in two 5-min blocks (laser on blocks); each laser on block was followed by 5 min without stimulation (laser off blocks). Sessions were video recorded with standard video cameras (25/30 fps); a mirror was placed to allow for observation of the rat's mouth regardless of position. A trained experimenter scored the videos offline, and calculated the % of time each rat spent feeding during laser off and laser on blocks.

Histologic analyses

For *in vitro* experiments, the frontal part of the brain containing the amygdala was trimmed and placed in 4% PFA (pH 8.4) in 0.1 M phosphate buffer; for all other experiments, rats were transcardially perfused with heparinized physiological solution (0.9% NaCl) followed by 4% PFA. Brains were immersed in 4% PFA overnight, then cryoprotected in 20% and 30% sucrose in 0.1 M phosphate buffer for 24 h each before being flash-frozen in isopentane at −80°C. Coronal sections containing the CeA or LPBN (40-µm thickness) were sliced using a cryostat (CM3050S, Leica Microsystems). Slices were collected directly to microscope slides [CeA-containing slices for FISH (fluorescence *in situ* hybridization), see below] and stored at −80°C, or stored in well-plates containing 0.05% Na-azide in 1 × PBS at 4°C until further processing. To better visualize mCherry-expressing axons at the LPBN level, immunohistochemical labeling was used to amplify the mCherry signal in a subset of brainstem slices. For this, free-floating slices were treated with 0.1% Triton X-100 in 1 × PBS, blocked with 4% normal donkey serum (Abcam) in 1 × PBS containing 0.1% Triton X-100 (blocking buffer) for 1 h, incubated overnight in mouse anti-mCherry (1:2000 in blocking buffer; BioLegend) and subsequently in donkey anti-mouse conjugated to Alexa Fluor 546 (1:1000 in blocking buffer; Invitrogen) for 2 h. In addition, for HSV1 injections and behavioral experiments, the detection of injection site and optic fiber placement, respectively, was assisted by immunohistochemical labeling for microglia; after the treatment with 0.1% Triton X-100 in 1 × PBS and the blocking step (as described above), free-

floating sections were incubated in goat anti-ionized calcium-binding adapter molecule 1 (anti-Iba1; 1:2000 in blocking buffer; Abcam) followed by donkey anti-goat conjugated to Alexa Fluor 647 (1:1000 in blocking buffer; Invitrogen) for 2 h. All incubation steps were performed at room temperature. A mounting medium containing DAPI (Fluoromount-G, Invitrogen) was applied to stain for cell nuclei. Mounted sections were cover-slipped and viewed with a fluorescence microscope (BX51, Olympus); anatomical landmarks were identified with the assistance of a brain atlas (Paxinos and Watson, 2007). For FISH experiments, only data from rats in which the HSV1 vector was injected within the LPBN was included in subsequent analyses. For all experiments involving intra-CeA AAV injections, a prerequisite for inclusion in subsequent analyses was the identification of mCherry+ somata and mCherry+ axons in the CeA and LPBN, respectively. In addition, for *in vivo* electrophysiological and behavioral experiments, only experiments for which the tetrode tip was positioned within the LPBN and optic fiber tips were placed dorsally to the LPBN, respectively, were further analyzed.

FISH was performed using hybridization chain reaction (HCR) protocols (Molecular Instruments). Sections containing the CeA were washed and incubated in 1 × PBS (10 min at room temperature), dried for 10 min at 55°C, followed by incubation in 4% PFA (15 min at 4°C, pH 8.4). After dehydration in ethanol (50%, 70%, 96%, and 100%, at room temperature), sections were incubated in proteinase K (10 µg/ml in PBS; Roth) for 10 min at 37°C, then washed with PBS. In separate sections, RNA probes were used to label cells expressing mRNA for CaMKIIα and somatostatin, the vesicular GABA transporter (VGAT) and corticotropin-releasing hormone (CRH), or for somatostatin only. For fluorescence labeling of mRNA, HCR amplifiers were conjugated to Alexa Fluor 488 (anti-VGAT and anti-somatostatin probes) or Alexa Fluor 647 (anti-CaMKIIα, anti-CRH, and anti-somatostatin probes). Sections were pretreated with probe hybridization buffer for 10 min, and then incubated overnight in a solution containing RNA probes (0.4 pmol of probe in hybridization buffer), at 37°C. Sections were washed with HCR probe wash buffer and subsequently with mixtures of wash buffer and 5×SSC-T (5 × saline-sodium citrate buffer with 0.1% Tween 20; Sigma-Aldrich) in proportions of 75%/25%, 50%/50%, and 25%/75%, followed by incubation in 100% 5×SSC-T, at 37°C (15 min per step). Sections were incubated for 30 min in HCR amplification buffer, then treated overnight with a mixture of preactivated HCR amplifiers (6 pmol) in HCR amplification buffer, at room temperature. Sections were incubated in a DAPI solution (1:1000 in 1 × PBS; Abcam), then washed with 1 × PBS. An antifade reagent (ProLong Gold, Invitrogen) was added before coverslip placement. Fluorescent images of the right CeA (ipsilateral to the HSV1 injection site; 6–11 sections per rat, equally spaced along the CeA's rostrocaudal axis) were captured using an inverted confocal microscope (Leica TCS SP5, 20×/0.70 N.A. glycerol immersion objective, 2048 × 2048 pixels, 30- to 40-µm z-stacks with 3-µm intervals), using the Leica Application Suite Advanced Fluorescence software (Leica Microsystems). The excitation laser lines used were 405, 488, 561, and 633 nm. Photograph multiplier tubes and hybrid detectors were used to detect emitted light; pinhole size was adjusted for each channel (100–150 µm). Images were analyzed offline using Fiji ImageJ (V1.53c). The cell-counting plugin was used to mark identified mCherry-labeled somata with DAPI-stained nuclei within the CeA, and to quantify the number of mCherry+ cells co-labeled for VGAT, CRH, CaMKIIα, or somatostatin mRNA.

Experimental design and statistical analyses

For molecular characterization of CeA^{CAM}-LPBN neurons using FISH, the ratio of retrogradely-labeled CeA^{CAM} somata expressing VGAT, CRH, CaMKIIα, and somatostatin are reported. The distribution of response latency parameters in *in vitro* electrophysiology experiments are given as the % of analyzed cells. When analyzing the effects of drugs on PSCs recorded *in vitro*, postdrug values were normalized to baseline (100%). For analyses involving *in vivo* MUA responses to sciatic nerve stimulation, the effect of laser stimulation on firing rate (normalized as % change from the laser off condition) was calculated separately for weak nerve stimulation, and for the early and late LPBN response components evoked by strong nerve stimulation. As laser effects did not significantly differ between these three response categories (see Results), they were averaged to produce a pooled laser effect per recording site. For *in vivo* single-unit data, firing rates were compared between the laser off and laser on conditions.

Statistical analyses were performed with GraphPad Prism (GraphPad Software), and p-values < 0.05 were considered statistically significant. All tests were two-tailed, unless otherwise specified, and p-values were corrected for multiple comparisons when appropriate. Statistical comparisons were performed based on the specific research question and the number of comparisons. Pairwise comparisons were performed using the paired-samples t test, or the Wilcoxon matched-pairs test when normality could not be assumed (as evaluated by the Shapiro–Wilk test). Slope comparison was performed with a linear regression analysis. For experiments involving two independent variables, a two-way ANOVA was performed, followed by the Holm–Sidak multiple comparisons *post hoc* test. For threshold tests, a mixed effects model analysis, followed by the Holm–Sidak multiple comparisons test where appropriate, was used to test the following hypotheses: (1) threshold values for the left paw on day 0 would be lower than for all other day-paw combinations (capsaicin effect); (2) laser stimulation would increase withdrawal values in the AAV-ChR2 group but not in the AAV-mCherry group (group × laser interaction); (3) the effect of laser stimulation would be influenced by capsaicin treatment (group × laser × capsaicin interaction). Group sizes were calculated using SigmaPlot 12 (Systat Software Inc.), taking into account the type and number of planned comparisons, as well as the expected variability, based on previous experience and pilot data. Data are expressed as mean ± SEM, unless stated otherwise.

Results

Almost all LPBN-projecting CeA neurons express CaMKIIα, VGAT, and somatostatin, but not CRH

Following intra-LPBN injections of HSV1-CMV-mCherry or HSV1-CaMKIIα-mCherry, LPBN-projecting neurons could be identified throughout the rostrocaudal axis of the CeA, with most CeA-LPBN neurons concentrated in the medial CeA, and no retrogradely labeled neurons observed in the lateral or basolateral amygdala (Fig. 1*A*). Using a combination of FISH and confocal microscopy, we genetically characterized CeA-LPBN neurons. Almost all LPBN-projecting CeA neurons labeled with HSV1-CMV-mCherry ($n = 4$ rats; total of 125 cells in 20 slices) expressed mRNA for CaMKIIα (90.4 ± 3.2%) and somatostatin (98.4 ± 2.4%; see example in Fig. 1*B*). Almost all CeA neurons labeled with HSV1-CaMKIIα-mCherry expressed VGAT mRNA (99 ± 0.6%), while CRH mRNA was detected in a minority of CeA^{CAM}-LPBN neurons (20.2 ± 3.5%), and was mostly observed in cell clusters concentrated in the ventrolateral CeA, where mCherry+ somata were sparse ($n = 5$ rats; Fig. 1*C*,*E*). Similarly to the general population of CeA-LPBN neurons, the vast majority of CeA^{CAM}-LPBN neurons (90.1 ± 2.7%; $n = 6$ rats) was co-labeled for somatostatin mRNA (Fig. 1*D*,*E*).

CeA^{CAM} neurons form GABAergic synapses throughout the LPBN

We next set out to examine whether CeA^{CAM} neurons form functional GABAergic synapses with LPBN neurons, and determine the anatomic distribution of CeA^{CAM} inputs within the LPBN. For this, AAV-ChR2 was bilaterally injected into the CeA of rats (Fig. 1*F*); after a gene expression period of at least four weeks, acute brainstem slices containing the LPBN were prepared. mCherry+ CeA axons could be observed throughout the LPBN, with the highest density in the area directly dorsal to the superior cerebellar peduncle, but not confined to specific LPBN subregions. LPBN neurons located within areas rich in

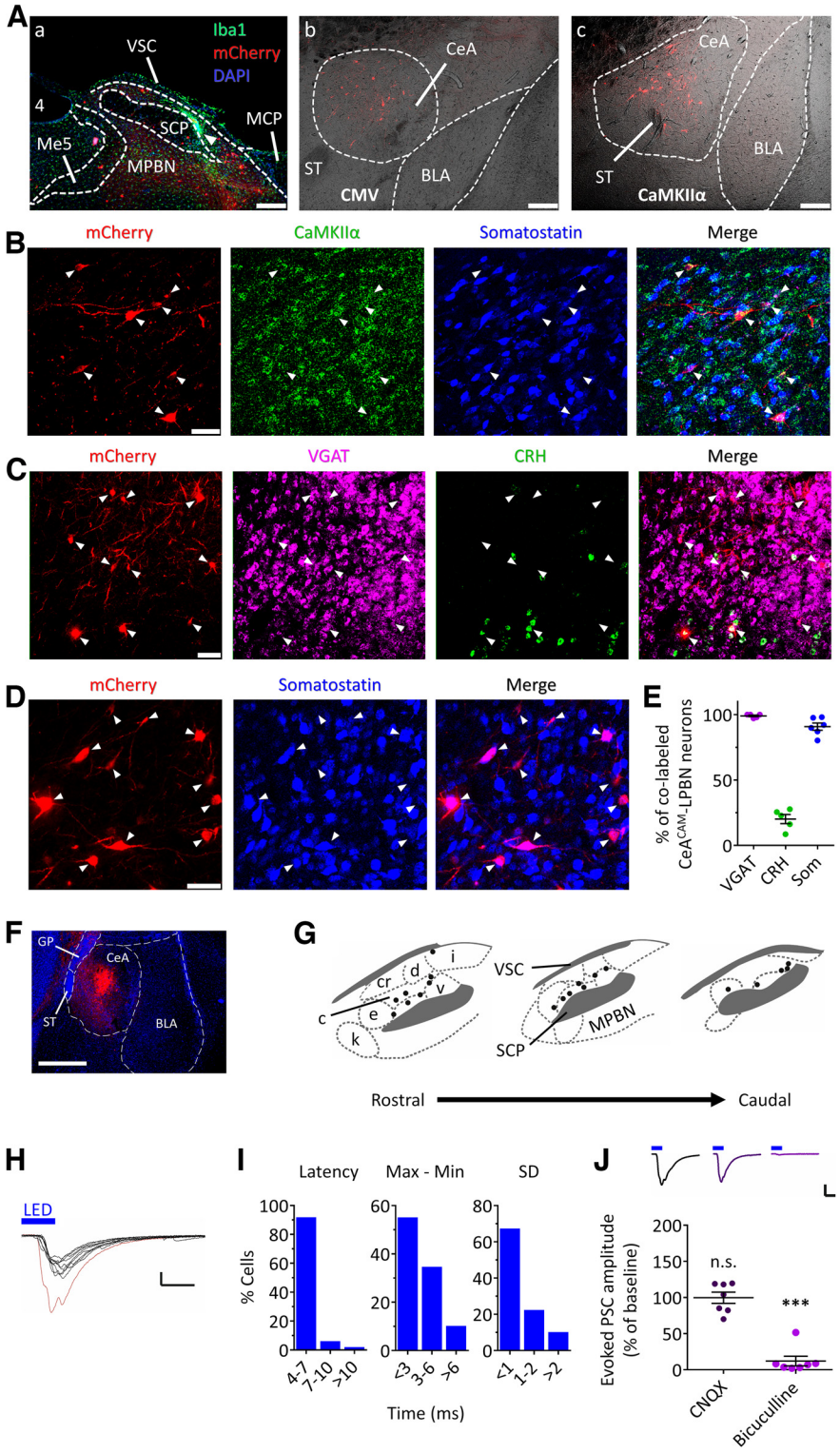

Figure 1. Anatomical, molecular, and electrophysiological characterization of CeA^{CAM}-LPBN projections. ***A***, Retrograde labeling of LPBN-projecting neurons was achieved by injection of HSV1-CMV-mCherry or HSV1-CaMKIIα-mCherry into the LPBN. Arrowhead (***a***) points to injection site, identified by strong expression of the microglia marker Iba1 (green). Both for the general population of CeA-LPBN neurons labeled with HSV1-CMV-mCherry (***b***), and specifically for CaMKIIα+ CeA-LPBN neurons labeled with HSV1-CaMKIIα-mCherry (***c***), LPBN-projecting neurons (red) were observed in the CeA, mostly in the medial division. BLA = basolateral amygdala; MCP = medial cerebellar peduncle; Me5 = mesencephalic trigeminal nucleus; MPBN = medial parabrachial nucleus; SCP = superior cerebellar peduncle; ST = stria terminalis; VSC = ventral spinocerebellar tract; 4 = fourth ventricle. Scale bars: 250 μm. ***B***, Confocal microscopy images of genetically characterized CeA-LPBN neurons retrogradely labeled with HSV1-CMV-mCherry. Almost all labeled (>90%) mCherry+ CeA somata (red, marked by arrowheads) were co-labeled for CaMKIIα (green) and somatostatin (blue). ***C***, ***D***, Arrowheads point to the somata of mCherry+ CeA^{CAM}-LPBN neurons (red), retrogradely labeled using the HSV1-CaMKIIα-mCherry vector. Scale bars: 50 μm (***B–D***). ***E***, Summary of results from mCherry+ axons were targeted for whole-cell voltage-clamp recordings; blue light stimulation evoked PSCs in neurons located throughout the LPBN (Fig. 1*G*). Once a LPBN neuron showed a response to optogenetic stimulation, a blue light train (10 pulses at 10 Hz) was delivered. In most responsive LPBN neurons examined (49/55, 89.1%), light trains evoked PSCs with a failure rate of ≤10% (a representative example is shown in Fig. 1*H*). The median response latency in these neurons was 5.5 ms (interquartile range: 4.8–6.1 ms); the median range of latencies per train (maximum latency – minimum latency) was 2.7 ms (interquartile range: 2–9 ms); and the median SD of latencies per train was 0.9 ms (interquartile range: 0.6–1.2 ms). The distribution of latency parameters within the population of recorded LPBN neurons is summarized in Figure 1*I*. To further characterize CeA^{CAM}-LPBN synaptic transmission, we used a pharmacological approach. While PSC amplitude

←

CeA^{CAM}-LPBN neurons. For VGAT/CRH experiments, a total of 925 identified CeA^{CAM}-LPBN neurons were examined in 36 slices ($n = 5$ rats); for somatostatin (Som) experiments, a total of 922 CeA^{CAM}-LPBN neurons were examined in 53 slices ($n = 6$ rats). ***F***, A typical example of a confirmed AAV-ChR2 injection site within the CeA. Following virus injection, mCherry (red) was expressed in CaMKIIα+ neurons, shown on the background of DAPI staining (blue). Scale bar: 500 μm. BLA = basolateral amygdala; GP = globus pallidus; ST = stria terminalis. ***G***, In acute brainstem slices, LPBN neurons (black dots) responding to optogenetic stimulation of CeA^{CAM} axons with PSCs ($n = 20$ representative cells from 12 rats) could be identified in multiple subdivisions of the LPBN: c = central; cr = crescent; d = dorsal; e = external; i = internal; k = Kölliker-Fuse; v = ventral; MPBN = medial parabrachial nucleus; SCP = superior cerebellar peduncle; VSC = ventral spinocerebellar tract. ***H***, A typical example of superimposed PSCs elicited in LPBN neurons on 10 × 10 Hz photostimulation of CeA^{CAM} axons in acute brainstem slices. Response to the first light pulse is shown in red. Scale bars: 100 pA and 10 ms. ***I***, Summary of PSC latency data from 49 LPBN neurons responding to 10 × 10 Hz photostimulation train with a failure rate of ≤10%. Bar graphs show the % of cells responding with particular latencies to the first light pulse, the range of latencies per train (maximum latency – minimum latency), and the SD of response latencies per train. ***J***, Individual traces (top; scale bars: 300 pA and 10 ms) and group data (bottom) showing the effects of CNQX and bicuculline on LPBN PSCs evoked by photostimulation of CeA^{CAM}-LPBN synapses. PSC amplitudes were normalized to the mean amplitude of PSCs evoked during the baseline period, before drug application (black trace). PSC amplitudes were unchanged following bath application of 10 μM CNQX (purple trace; 99.7 ± 7.7% of baseline; $p > 0.99$); n.s. = non significant. In contrast, bath application of bicuculline (10 μM) resulted in a strong reduction in PSC amplitudes (magenta trace; 12 ± 6.7% of baseline; ***$p < 0.0005$).

was not affected by CNQX application (99.7 ± 7.7% of baseline; $t_{(6)} = -0.04$, $p > 0.99$, $n = 7$ cells from 6 rats; Bonferroni-corrected one-sample t test), PSCs were virtually abolished following bicuculline application (12 ± 6.7% of baseline; $t_{(6)} = -9.33$, $p = 0.0004$; Bonferroni-corrected paired t test, comparison with post-CNQX responses; Fig. 1*J*). Taken together, these results indicate that CeA^{CAM} axons form monosynaptic connections throughout the LPBN, and likely affect LPBN activity through activation of postsynaptically-expressed $GABA_A$ receptors (Mody and Pearce, 2004; Thomson and Jovanovic, 2010; Shrivastava et al., 2011).

Optogenetic stimulation of CeA^{CAM}-LPBN projections attenuates population LPBN responses to putative Aδ- and C-fiber inputs in a $GABA_A$ receptor-dependent manner

Based on their inhibitory nature, we hypothesized that optogenetic stimulation of CeA^{CAM}-LPBN projections would attenuate responses of LPBN neurons to peripheral noxious stimuli *in vivo*. Since noxious stimuli mostly activate Aδ- and C-fiber primary afferents, we sought to quantify the effect of CeA^{CAM}-LPBN stimulation on LPBN responses to each of these inputs. For this, we delivered weak (1 V) and strong (15 V) electrical pulses to the sciatic nerve of rats that previously received intra-CeA AAV injections, and analyzed MUA responses recorded from the LPBN (Fig. 2*A*,*B*). Weak nerve stimulation typically evoked a phasic population response, peaking ~15 ms after nerve stimulation (Fig. 2*C*), consistent with Aδ-fiber activation. Strong nerve stimulation produced a more complex population response in the LPBN, consisting of both the phasic component observed in weak stimulation trials (early component, driven primarily by Aδ-fiber input), and an additional late component (onset >80 ms after nerve stimulation, with a typical duration of 100–200 ms), attributable to C-fiber input (Fig. 2*B*,*D*). In AAV-ChR2-injected animals, optogenetic stimulation of CeA^{CAM}-LPBN axons often induced a marked reduction in LPBN population responses to weak nerve stimulation (Fig. 2*C*,*E*), as well as to both response components evoked by strong nerve stimulation (Fig. 2*D*,*F*). LPBN responses to weak and strong Aδ-fiber activation by 1- and 15-V stimulation, respectively, were reduced to a similar degree by optogenetic stimulation (23.5 ± 6.5% and 24.2 ± 5.3% reduction in the early component compared with laser off, respectively; $t_{(14)} = 0.1$, $p > 0.99$; Bonferroni-corrected paired t test; $n = 15$ recording sites in 12 AAV-ChR2 rats). Likewise, there was no significant difference in the effect of laser stimulation when comparing the early and late LPBN response components evoked by strong nerve stimulation (24.2 ± 5.3% and 13 ± 5.4% reduction compared with laser off, respectively; $t_{(14)} = 2.46$, $p = 0.055$; Bonferroni-corrected paired t test; Fig. 2*G*). Overall, laser stimulation of CeA^{CAM}-LPBN axons induced a significant reduction in responses to sciatic nerve stimulation in AAV-ChR2 rats as compared with AAV-mCherry controls (20.2 ± 4.4% and 0.3 ± 4.2% reduction compared with laser off, respectively; $t_{(21)} = -3$, $p = 0.008$; independent samples t test; Fig. 2*H*).

In a separate cohort of AAV-ChR2 rats, the effect of optogenetic stimulation of CeA^{CAM}-LPBN axons was abolished by intra-LPBN microinjection of bicuculline (31.7 ± 7% reduction and 2.8 ± 7.3% increase compared with laser off before and after bicuculline injection, respectively), but not by intra-LPBN microinjections of saline (33.9 ± 5.1% and 28.7 ± 4.2% reduction compared with laser off before and after saline injection, respectively; Fig. 2*I*). A two-way ANOVA revealed a significant drug × time interaction ($F_{(1,10)} = 13.4$, $p = 0.004$), and a *post hoc* Holm–Sidak test showed that the effect of optogenetic stimulation was significantly affected by intra-LPBN injection of bicuculline ($p = 0.0002$), but not saline ($p = 0.37$; $n = 6$ recording locations from 5 rats per group). Also for these recordings, preinjection laser effects were similar for LPBN responses evoked by 1-V (42.8 ± 8.3% reduction compared with laser off) and 15-V (early component; 30.9 ± 4% reduction; $t_{(11)} = 1.69$, $p = 0.24$) nerve stimulation, as well as for the early and late (24.8 ± 4.9% reduction) components evoked by 15-V stimulation ($t_{(11)} = 1.16$, $p = 0.54$; Bonferroni-corrected paired t tests). Taken together, these results show that optogenetic stimulation of CeA^{CAM}-LPBN axons inhibits LPBN responses to nociceptive inputs relayed by Aδ- and C-fibers to a similar degree, and that this inhibition is $GABA_A$ receptor-dependent.

Optogenetic stimulation of CeA^{CAM}-LPBN projections inhibits the responses of LPBN neurons to noxious mechanical, thermal, and chemical stimulation *in vivo*

Since optogenetic stimulation of CeA^{CAM}-LPBN projections attenuated LPBN neurons to Aδ- and C-fiber input, we hypothesized that it would be effective in inhibiting LPBN responses to various pain modalities. To test this hypothesis, extracellular activity recorded from the LPBN of anaesthetized AAV-ChR2 rats was spike-sorted offline (Fig. 3*A*), and responses of single LPBN units to noxious mechanical pressure (pinch), radiant heat (IR pulse), or intraplantar capsaicin injection into the contralateral (left) hindpaw were compared between the control condition (laser off) and during optogenetic stimulation (laser on).

To examine how activation of CeA^{CAM}-LPBN synapses would affect LPBN responses to mechanical pressure, pinches of varying intensities were applied to the hindpaw using calibrated forceps. Pinch intensities in laser off and laser on trials were yoked within each experiment (Fig. 3*B*). In the laser off control condition, LPBN neurons typically showed a marked increase in firing rate during the application of pinches, with higher forces eliciting more spikes (Fig. 3*C*). Pinch-evoked responses were substantially reduced in the laser on condition, where pinches were delivered during optogenetic stimulation of CeA^{CAM}-LPBN axons (Fig. 3*D*). A repeated-measures two-way ANOVA revealed significant main effects of force ($F_{(4,76)} = 10.2$, $p < 0.0001$) and laser condition ($F_{(1,19)} = 9.5$, $p = 0.0062$) on the firing rate of LPBN neurons, but no significant interaction ($F_{(4,76)} = 2$, $p > 0.1$, $n = 20$ neurons from 10 rats). On average, the rate of pinch-evoked firing was reduced by 37.5 ± 7.5% in the laser on condition compared with the laser off condition (Fig. 3*E*). A linear regression analysis confirmed that the laser on and laser off slopes were not significantly different from one another ($F_{(1,196)} = 0.2$, $p = 0.66$). These results indicate that the activation of CeA^{CAM}-LPBN axons dampens LPBN responses to noxious mechanical pressure without affecting the slope of the stimulus-response curve.

Neuronal LPBN responses to thermal stimulation were evoked by application of radiant heat (IR pulses, 5 s in duration). Heat-evoked responses were typically observed 4–6 s after IR pulse onset (Fig. 3*F*), and were significantly attenuated in the laser on condition (51.3 ± 11.3% reduction in firing rate compared with the laser off condition; Wilcoxon, $p = 0.0024$, $n = 13$ neurons from 7 rats; Fig. 3*G*,*H*).

To examine how CeA^{CAM} input would modulate LPBN responses to noxious chemical stimulation, the firing rate of LPBN neurons was examined 30–600 s after capsaicin injection, during alternating laser off and laser on blocks (Fig. 3*I*). Capsaicin-evoked activity was significantly lowered by optogenetic stimulation of CeA^{CAM}-LPBN axons (28.2 ± 9.5% reduction compared with laser off blocks; Wilcoxon, $p = 0.012$, $n = 23$ neurons from 13 rats; Fig. 3*J*).

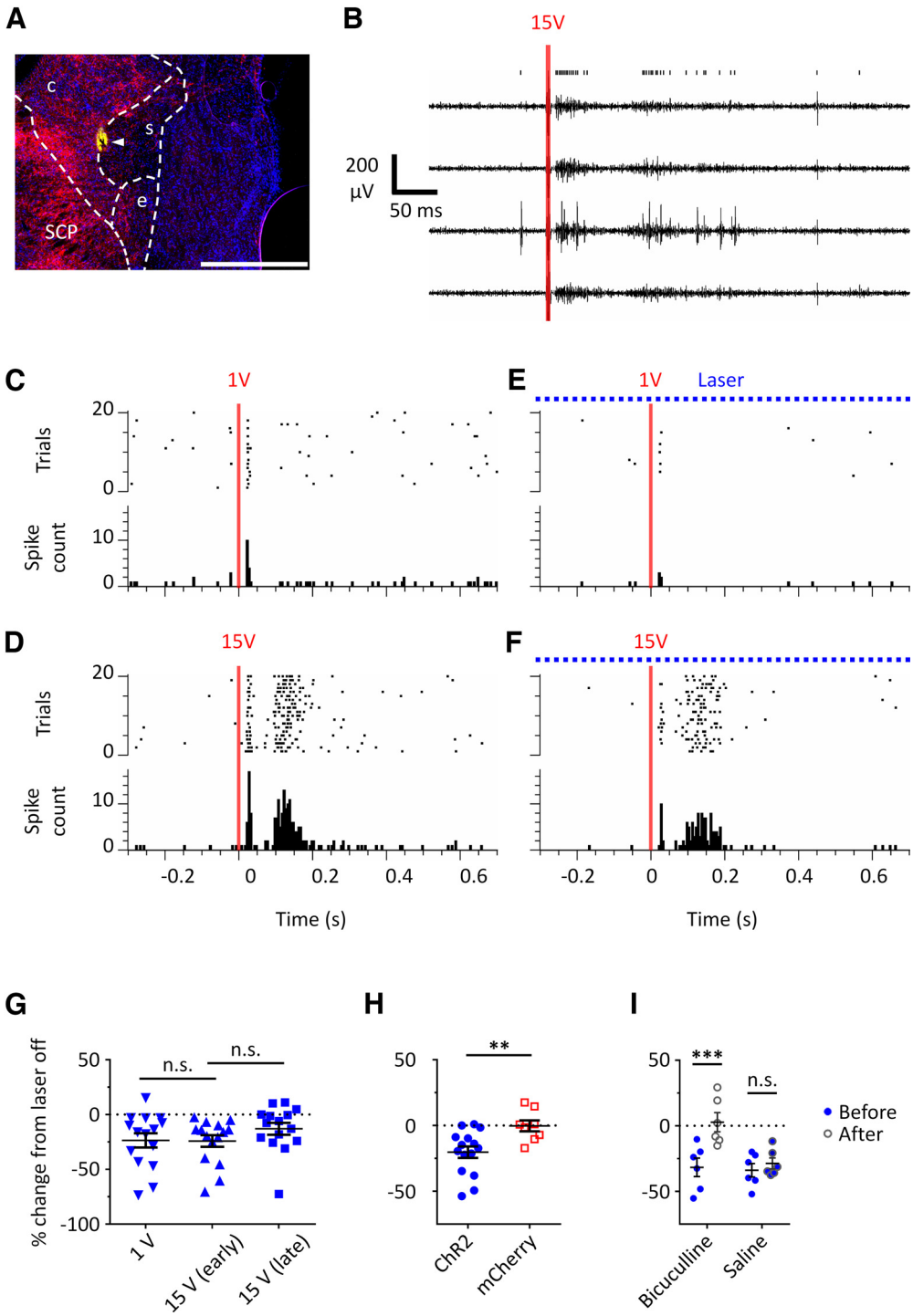

Figure 2. In anaesthetized rats, optogenetic stimulation of CeA^{CAM}-LPBN projections dampens population LPBN responses to putative Aδ- and C-fiber inputs. ***A***, Position of a tetrode tip (yellow) within the LPBN. mCherry+ axons of CeA^{CAM} neurons are shown in red; DAPI is shown in blue. Scale bar: 500 μm. SCP = superior cerebellar peduncle. LPBN divisions: c = central; e = external; s = superior. ***B***, Example of LPBN MUA response to noxious electrical sciatic nerve stimulation (15-V square pulse, 0.5 ms in duration; vertical red line). Nerve stimulation evoked multiple spikes confined within short time windows, in stark contrast to the low baseline firing rate. Ticks indicate suprathreshold spike events extracted from the MUA signal of at least one of four recording channels. ***C–F***, Histograms and raster plots showing example LPBN population responses to strong (15 V) and weak (1 V) electrical stimulation of the contralateral (left) sciatic nerve (0.5-ms square pulses) in a rat injected with AAV-ChR2. In the laser off condition (***C***, ***D***), the response to weak (1 V) nerve stimulation (***C***) evoked a phasic short-latency response; strong nerve stimulation evoked a similar early response, followed by a late response component with an onset latency >80 ms (***D***). Optogenetic stimulation of CeA^{CAM}-LPBN axons inhibited the response to weak nerve stimulation (***C***, ***E***), as well as both components of the response to strong nerve stimulation (***D***, ***F***). ***G***, In AAV-ChR2 rats, laser stimulation resulted in a similar reduction in firing evoked by weak or strong activation of Aδ-fibers (1 V compared with the early response to 15-V stimulation; $p > 0.99$; $n = 15$ recording sites in 12 rats). Similarly, there was no significant difference in the effect of optogenetic stimulation when comparing strong Aδ-fiber activation to C-fiber activation (early and late responses to 15-V stimulation; $p = 0.055$). ***H***, On average, laser stimulation reduced LPBN responses to sciatic nerve stimulation in AAV-ChR2 rats, but not AAV-mCherry rats ($n = 8$ recording sites in 6 rats; $^{**}p = 0.008$). ***I***, In a separate cohort of AAV-ChR2 rats, the effect of laser stimulation on LPBN responses could be abolished by intra-LPBN injection of bicuculline ($^{***}p = 0.0002$), but not saline ($p = 0.37$). Dashed line in ***G–I*** (0% change) indicates the mean response in laser off trials. n.s. = non significant.

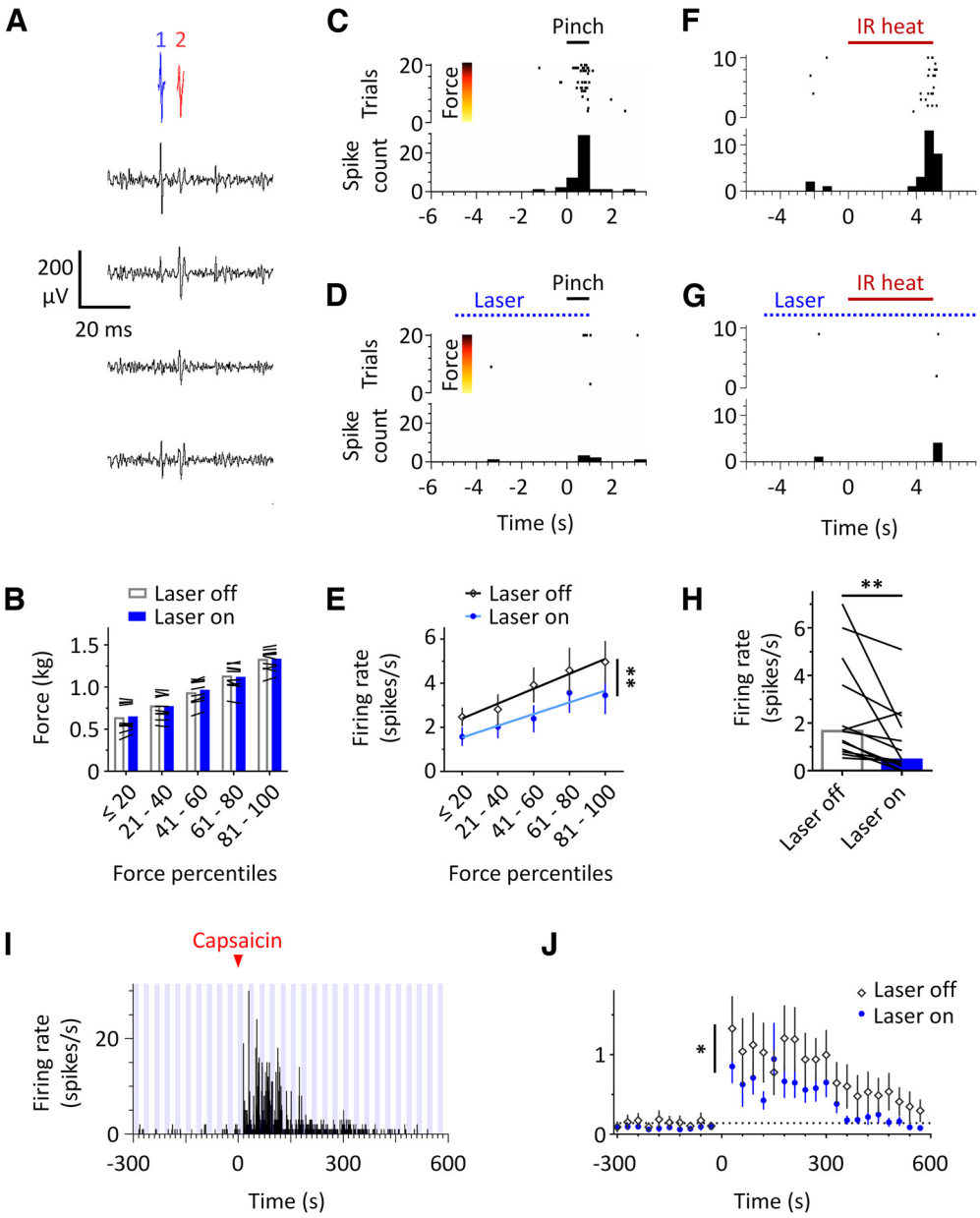

Figure 3. Optogenetic stimulation of CeA^{CAM}-LPBN projections dampens the response of LPBN neurons to noxious mechanical, thermal, and chemical stimuli of the contralateral (left) hindpaw in anaesthetized rats. ***A***, Example of spike sorting process. In this case, two distinct units could be separated according to their distinct contribution to the waveforms recorded by the tetrode's four sensors. ***B***, Forces of hindpaw pinches delivered in the control condition (laser off) and during optogenetic stimulation of CeA^{CAM}-LPBN axons (laser on), arranged by percentiles of force. For each percentile range, each black line represents one rat. Bars show the mean absolute force of each percentile range across animals. ***C***, ***D***, Example peristimulus time histograms and raster plots of a LPBN neuron responding to hindpaw pinch, in alternating laser off (***C***) and laser on trials (***D***). In the raster, trials are ordered by force applied, from lowest (1) to highest (20). ***E***, Summary of neuronal responses to pinch during laser off and laser on trials. Evoked firing was significantly lower in laser on trials compared with laser off (**$p = 0.0062$; $n = 20$ neurons from 10 rats). Linear regression curves are shown for each condition. ***F***, ***G***, Example histograms and raster plots of a LPBN neuron responding to hindpaw-directed radiant heat produced by a 5-s IR light pulse, in laser off (***F***) and laser on (***G***) trials. ***H***, Overall, heat-evoked firing rate was significantly reduced in the laser on condition, compared with laser off (**$p = 0.0024$; $n = 13$ heat-responsive neurons from 7 rats). Lines show average firing rates for each recorded neuron (interquartile range: 0.9–4.2 and 0.3–2.1 spikes/s), and bars show median firing rate per condition (1.7 and 0.5 spikes/s for the laser off and laser on conditions, respectively). ***I***, Example histogram showing the firing of a LPBN neuron (1-s bins). Like most nociceptive LPBN neurons, this neuron exhibited low spontaneous firing rate (<0.2 spikes/s) during the 5-min baseline period. Firing rate substantially increased following capsaicin administration (time 0, red arrowhead), and was higher during laser off blocks (mean of 2.39 spikes/s) compared with the laser on blocks (0.99 spikes/s; blue bars). ***J***, Average firing rate of all capsaicin-responsive LPBN neurons ($n = 23$ neurons from 13 rats), in laser off and laser on blocks. Dashed line indicates the average firing rate in laser off blocks during the baseline period. Firing rate in the period of 30–600 s postcapsaicin was significantly lower during laser on blocks (interquartile range: 0.1–0.6, median: 0.2 spikes/s) compared with laser off blocks (interquartile range: 0.2–0.7, median: 0.4 spikes/s; *$p = 0.012$).

Activation of CeA^{CAM}-LPBN projections attenuates nocifensive responses to mechanical and thermal stimuli in behaving rats

Given that our electrophysiological data show that optogenetic stimulation of CeA^{CAM}-LPBN projections inhibits neuronal LPBN responses to noxious peripheral stimuli regardless of submodality, we hypothesized that it would also attenuate nocifensive responses to both mechanical and heat stimulation, whether in baseline conditions or in a state of capsaicin-mediated hypersensitivity. To test this hypothesis, rats received intra-CeA injections of

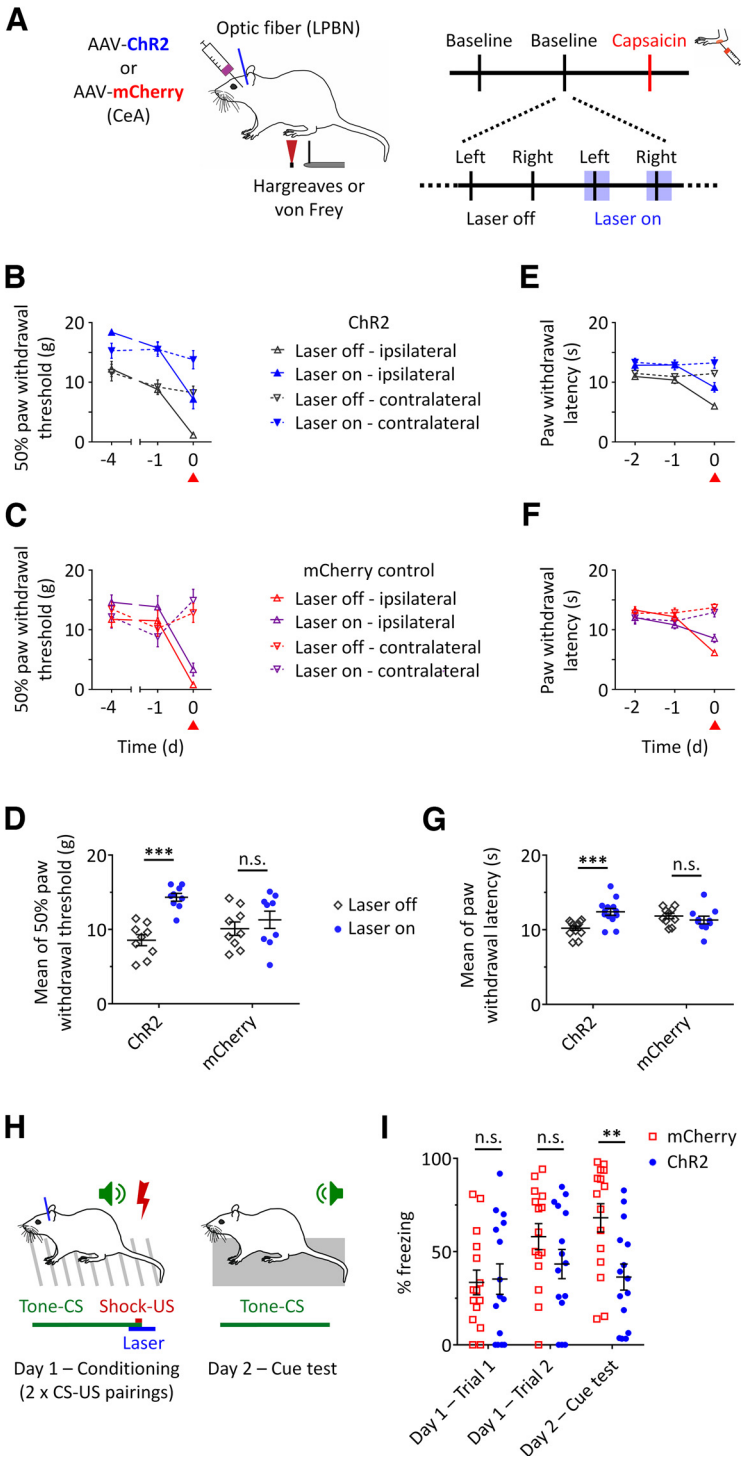

Figure 4. Optogenetic stimulation of CeA^{CAM}-LPBN projections in behaving rats reduces nocifensive responses and hampers aversive learning involving a noxious unconditioned stimulus. ***A***, Experimental design for examining nocifensive responses to mechanical (von Frey) and thermal (Hargreaves) stimulation of the hindpaws. Rats received bilateral intra-CeA injections of either AAV-ChR2 or the control vector AAV-mCherry, and optic fibers were implanted above the LPBN. In each session, each paw was stimulated with laser stimulation off or on (intermingled trials). On the last day of testing (day 0), the test session was preceded by a capsaicin injection into the left hindpaw. ***B***, ***C***, Time course of von Frey experiment for mechanical sensitivity, for the AAV-ChR2 group (***B***) and for the AAV-mCherry group (***C***). Measurements were taken over 3 d. The red arrowhead indicates capsaicin injection into the left hindpaw. ***D***, The mean 50% paw withdrawal threshold was significantly higher in the laser on condition as compared with the laser off condition in the AAV-ChR2 group (***$p < 0.0001$), but not in the AAV-mCherry group ($p = 0.13$). ***E***, ***F***, Time course of Hargreaves experiment for heat sensitivity in the AAV-ChR2 group (***E***) and in the AAV-mCherry control group (***F***). Measurements were taken over 3 d. The red arrowhead indicates capsaicin injection into the left hindpaw. ***G***, On average, paw withdrawal latencies were significantly higher in the laser on condition as compared with the laser off condition in the AAV-ChR2 group (***$p = 0.0004$), but not in the AAV-mCherry group ($p = 0.35$). ***H***, Experimental design for examining the effect of CeA^{CAM}-LPBN stimulation on unconditioned and conditioned freezing in a threat conditioning paradigm. In the conditioning session, a tone-CS (2 kHz at 70 dB, for 10 s) was paired with a co-terminating electrical shock-US (1 mA for 0.5 s; 2 pairings, 5-min intertrial interval). To inhibit shock-evoked LPBN responses in the AAV-ChR2 group, laser stimulation was delivered to the LPBN for 2 s in each trial, beginning 1 s before shock onset. On the next day, animals underwent a "cue test" session, in which they were placed in a novel chamber, and the tone-CS was presented for three consecutive minutes. The % of time rats spent freezing following shocks was used as a measure of shock aversiveness, while the % of time spent freezing during tone presentation was used as a measure of the previously-acquired aversive learning. ***I***, Both groups showed similar amount of freezing following shock presentations (conditioning trials 1 and 2; $p = 0.86$ and $p = 0.3$, respectively). During the cue test, rats in the AAV-ChR2 group showed significantly less conditioned freezing compared with the AAV-mCherry group (**$p = 0.009$; $n = 15$ rats per group). ***D***, ***G***, ***I***, n.s. = non significant.

either AAV-ChR2 or the control vector AAV-mCherry, and were subsequently tested in either the von Frey test or the Hargreaves test, to assess mechanical or thermal sensitivity, respectively. For both tests, measurements were taken on two baseline days, followed by an additional measurement after a capsaicin injection into the left hindpaw. Each session consisted of laser off and laser on trials (Fig. 4*A*).

Withdrawal thresholds in the von Frey test are shown for AAV-ChR2 and AAV-mCherry rats ($n = 9$ per group) in Figure 4*B*,*C*. A mixed effects model analysis revealed a significant effect of capsaicin ($F_{(5,80)} = 48.4$, $p < 0.0001$), and a *post hoc* Holm–Sidak test showed that withdrawal thresholds of the left paw on day 0 were significantly lower than for all other day-paw combinations ($p < 0.0001$ for all). The group × laser interaction was significant ($F_{(1,80)} = 21.2$, $p < 0.0001$), with paw withdrawal thresholds being significantly higher in the laser on condition compared with the laser off condition in the AAV-ChR2 group ($14.3 \pm 0.5 \times g$ compared with $8.5 \pm 0.7 \times g$; $p < 0.0001$), but not in the AAV-mCherry group (11.3 ± 1.2 g compared with 10.1 ± 0.9 g; $p = 0.09$; Holm–Sidak; Fig. 4*D*). The group × laser × capsaicin interaction was not significant ($F_{(5,80)} = 0.6$, $p = 0.67$), indicating that the effect of optogenetic stimulation was not altered by the presence of mechanical hypersensitivity.

Paw withdrawal latencies to radiant heat in the AAV-ChR2 ($n = 13$) and AAV-mCherry ($n = 10$) groups, as measured by the Hargreaves tests, are shown in Figure 4*E*,*F*. A mixed effects model analysis revealed a significant effect of capsaicin ($F_{(5,105)} = 28.1$, $p < 0.0001$), with the mean withdrawal latency being significantly lower for the left hindpaw on day 0 compared with all other day-paw combinations ($p < 0.0001$ for all; Holm–Sidak). The group × laser interaction was significant ($F_{(1,105)} = 13.43$, $p = 0.0004$), and the Holm–Sidak *post hoc* test showed that paw withdrawal latencies were significantly higher in the laser

←

on condition compared with the laser off condition in the AAV-ChR2 group (12.4 ± 0.5 s compared with 10.2 ± 0.3 s; $p = 0.0004$), but not in the AAV-mCherry group (11.3 ± 0.5 s compared with 11.8 ± 0.4 s; $p = 0.35$; Fig. 4*G*). The group × laser × capsaicin interaction was not significant ($F_{(5,105)} = 1.3$, $p = 0.27$), indicating that the effectiveness of laser stimulation was not influenced by capsaicin-induced hypersensitivity to heat.

Taken together, these results show that optogenetic stimulation of CeA^{CAM}-LPBN projections produced an overall anti-nociceptive effect, in line with its inhibitory effect on nociceptive LPBN signaling.

Stimulation of CeA^{CAM}-LPBN projections during the presentation of a noxious unconditioned stimulus interferes with acquisition of aversive learning, but not with unconditioned freezing

Since LPBN neurons relay information to a number of downstream targets involved in pain aversion and aversive learning (see Discussion), we hypothesized that optogenetic stimulation of CeA^{CAM}-LPBN projections during the presentation of a noxious shock would interfere with the ability of this shock to induce unconditioned freezing, as well as its ability to act as a teaching signal in an aversive learning paradigm. To test these hypotheses, AAV-mCherry rats and AAV-ChR2 rats ($n = 15$ rats per group) were subjected to threat conditioning in which a tone-CS predicted the occurrence of a shock-US. The shock-US was presented on the background of laser stimulation, such that it would be expected to inhibit shock-evoked LPBN output in AAV-ChR2 rats (Fig. 4*H*). The level of freezing displayed by rats in response to the presentation of the shock-US on day 1 (conditioning session, two trials) and by the tone-CS on day 2 (cue test) served as a measure of shock aversiveness. A repeated measures two-way ANOVA revealed a significant main effect of time ($F_{(2,56)} = 6.47$, $p = 0.003$) and a significant time × group interaction ($F_{(2,56)} = 4.7$, $p = 0.014$), while the main effect of group was not significant ($F_{(1,28)} = 3.2$, $p = 0.083$). A *post hoc* Holm–Sidak test showed that the % of freezing was not significantly different between groups for both the first and second conditioning trials ($p = 0.86$ and $p = 0.3$, respectively). In contrast, the AAV-ChR2 group exhibited significantly lower % conditioned freezing during the cue test ($p = 0.009$; Fig. 4*I*). These results suggest that activation of CeA^{CAM}-LPBN projections can reduce shock-evoked LPBN output to brain areas involved in aversive learning (e.g., the CeA).

CeA^{CAM} input to the LPBN reduces defensive behavior

We next sought to examine how stimulation of CeA^{CAM}-LPBN projections would affect defensive behavior. First, we quantified thigmotaxis behavior in AAV-ChR2 and AAV-mCherry rats ($n = 10$ per group) receiving continuous laser stimulation for 10 min in an open field arena. AAV-ChR2 rats showed significantly less thigmotaxis behavior compared with AAV-mCherry rats (69.7 ± 4.6% compared to 81.1 ± 1.8% of time spent in the wall area, respectively; $t_{(18)} = -2.31$, $p = 0.033$; unpaired *t* test; Fig. 5*A*,*B*). The total track length was similar for both groups (19.2 ± 3.5 and 22.4 ± 3.2 m in the AAV-mCherry and AAV-ChR2 group, respectively; $t_{(18)} = -0.68$, $p = 0.51$; unpaired *t* test; Fig. 5*C*), indicating that laser stimulation did not affect overall locomotion.

In a separate cohort of animals, we experimentally induced conditioned freezing to a context (conditioning chamber) and a tone that were previously paired with noxious shocks (Fig. 5*D*). As can be seen in Figure 5*E*,*F*, in the absence of laser stimulation, AAV-mCherry ($n = 7$) and AAV-ChR2 rats ($n = 6$) exhibited similar levels of freezing; however, upon laser stimulation, only AAV-ChR2 rats showed a reduction in freezing. When considering all test sessions (context and cue), a two-way repeated-measures ANOVA revealed a significant main effect of laser condition ($F_{(1,11)} = 11.7$; $p = 0.006$), as well as a significant laser × group interaction ($F_{(1,11)} = 25.5$, $p = 0.0004$), while the main effect of group was not statistically significant ($F_{(1,11)} = 1.4$, $p = 0.27$). A *post hoc* Holm–Sidak test confirmed that the amount of freezing was similar for both groups in the laser off condition (55.5 ± 7.2% and 64.1 ± 2.9% for the AAV-mCherry and AAV-ChR2 groups, respectively; $p = 0.41$), while AAV-ChR2 rats exhibited significantly less freezing in the laser on condition (31.4 ± 10.2%) compared with AAV-mCherry rats (61.8 ± 6.4%, $p = 0.013$; Fig. 5*G*). Taken together, these results indicate that the analgesic effect induced by CeA^{CAM} input to the LPBN is accompanied by reduced defensive behavior.

CeA^{CAM} input to the LPBN is rewarding and promotes feeding in sated rats

Inhibition of LPBN neurons was previously reported to have both anti-aversive and pro-appetitive effects (see Discussion). Therefore, we sought to examine whether optogenetic stimulation of CeA^{CAM}-LPBN projections would induce place preference, and whether place preference would be enhanced in pain model animals, in which laser stimulation would also attenuate pain sensation and its aversive impact. Therefore, we performed the RTPP test on three groups of rats: AAV-mCherry-Capsaicin ($n = 9$), AAV-ChR2-Capsaicin ($n = 8$; both of these groups receiving intraplantar capsaicin injection before testing), and AAV-ChR2-No pain ($n = 9$; who were only shortly handled before testing). Figure 6*A* shows example tracks from one AAV-ChR2-Capsaicin rat in the baseline and test sessions. This rat showed no clear preference to either compartment during the baseline session, when no laser stimulation was delivered. In contrast, in the test session, this animal showed a strong preference to the compartment in which laser stimulation was delivered. A summary of the results from all groups is shown in Figure 6*B*. A two-way repeated-measures ANOVA revealed a significant main effect of session ($F_{(1,23)} = 17.8$, $p = 0.0003$) and a significant session × group interaction ($F_{(2,23)} = 7.6$, $p = 0.003$), but no significant main effect of group ($F_{(2,23)} = 1.8$; $p = 0.19$). The Holm–Sidak multiple comparisons test confirmed that AAV-mCherry-Capsaicin rats spent a similar amount of time in the laser compartment during the baseline (51.3 ± 2.7%) and test sessions (47.6 ± 9.2%, $p = 0.57$). Conversely, both AAV-ChR2 groups showed an increased preference to the laser compartment in the test session compared with the baseline session (AAV-ChR2-Capsaicin: 78.1 ± 8.4% vs 45.9 ± 4%, $p = 0.0003$; AAV-ChR2-No pain: 72.5 ± 6.8% vs 53 ± 5.2%, $p = 0.012$). An additional Holm–Sidak test showed no difference between the AAV-ChR2-Capsaicin group and the AAV-ChR2-No pain group in either the baseline or test session ($p = 0.67$ for both; not corrected for the additional comparison), indicating that the rewarding effect of CeA^{CAM}-LPBN stimulation was not significantly affected by pain state.

Next, we examined the ability of CeA^{CAM}-LPBN stimulation to elicit feeding behavior in sated rats, using alternating laser on and laser off blocks (two of each kind, each 5 min in duration). In the AAV-mCherry group ($n = 21$), the % of time spent feeding was similar for laser off (interquartile range: 0–37%, median: 0%) and laser on blocks (interquartile range: 0–24.7%, median: 0%; $p > 0.99$). In contrast, in a subset of AAV-ChR2 rats ($n = 22$),

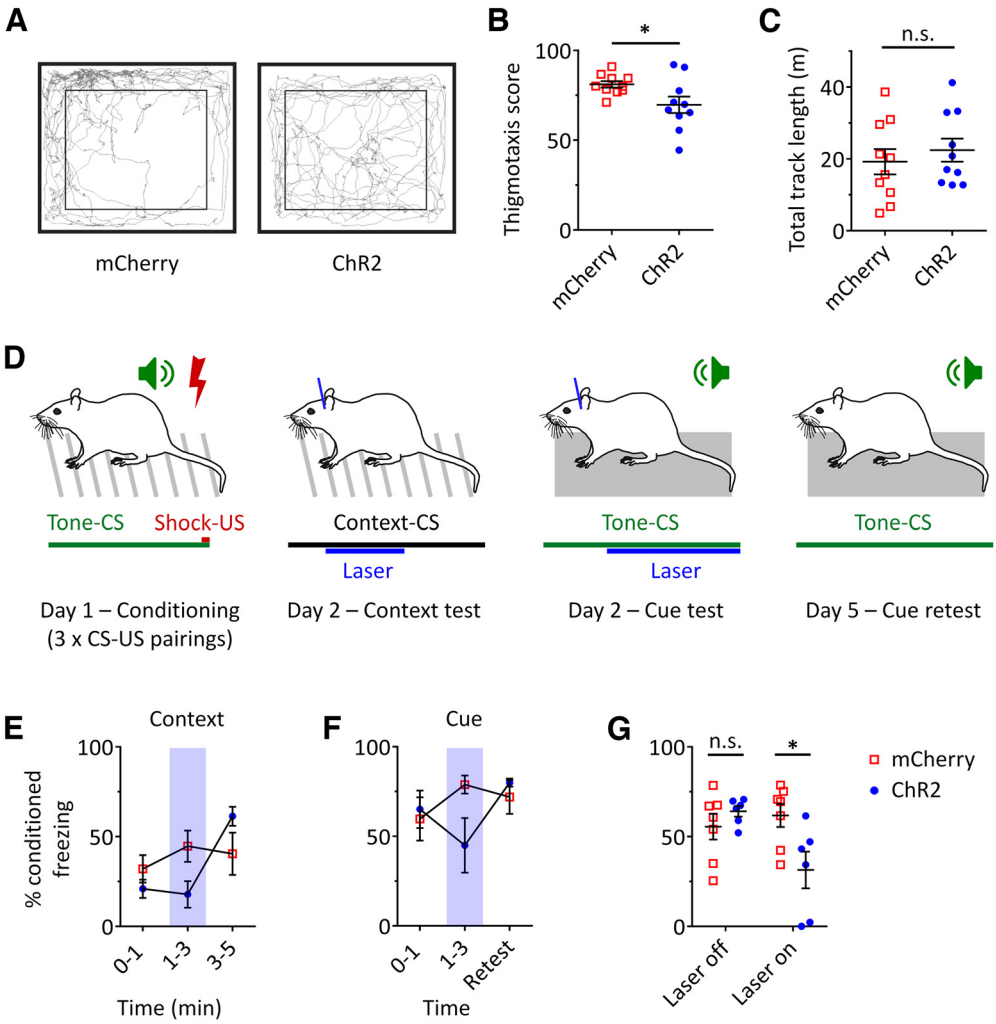

Figure 5. Optogenetic stimulation of CeA^{CAM}-LPBN projections attenuates defensive behaviors. ***A***, Example tracks of AAV-mCherry and AAV-ChR2 rats in the open-field arena (10-min free exploration, laser stimulation delivered throughout). The outer rectangle shows the "wall area" (15 cm on each side). ***B***, For each rat, the thigmotaxis score was defined as the % of time spent in the wall area. On average, AAV-ChR2 rats displayed significantly less thigmotaxis behavior compared with AAV-mCherry controls (*$p = 0.033$, $n = 10$ rats/group). ***C***, The total track length was similar for both groups ($p = 0.5$), indicating that activation of CeA^{CAM}-LPBN projections did not affect locomotion. ***D***, Experimental design for examining the effect of CeA^{CAM}-LPBN stimulation on the expression of conditioned freezing. In the conditioning session (day 1), a tone-CS (2 kHz at 70 dB, for 10 s) was paired with a co-terminating electrical shock-US (2 mA for 0.5 s; 3 pairings, 2-min intertrial interval). On day 2, animals underwent two types of test sessions: a "context test," in which they were placed in the conditioning chamber for 5 min (no stimuli delivered); and a "cue test," in which they were placed in a novel chamber, and the tone-CS was presented for three consecutive minutes. In each of these tests, laser stimulation was given for 2 min, beginning 1 min after test start. On day 5, rats underwent an additional cue test ("retest") which was identical to the first cue test, except that no laser stimulation was given. ***E***, ***F***, Time course of freezing behavior in AAV-mCherry ($n = 7$) and AAV-ChR2 rats ($n = 6$), in the context (***E***) and cue tests (***F***). Blue shadings represent the time periods in which laser stimulation was delivered. ***G***, Mean % conditioned freezing in laser on and laser off periods, across all test sessions (context and cue). When no laser stimulation was given, both groups spent similar time performing freezing behavior ($p = 0.8$). In contrast, when laser stimulation was delivered, AAV-ChR2 rats spent significantly less time freezing compared with AAV-mCherry rats (*$p = 0.01$). ***C***, ***G***, n.s. = non significant.

laser stimulation resulted in a marked increase in feeding (Fig. 6*C*). Overall, the % time spent feeding was significantly elevated in the AAV-ChR2 group during laser on blocks (interquartile range: 0–65.9%, median: 40.8%) compared with laser off blocks (interquartile range: 0–21.7%, median: 5.3%; $p = 0.013$; Bonferroni-corrected Wilcoxon's matched-pairs tests). Taken together, these results indicate that activation of CeA^{CAM}-LPBN projections produces an appetitive effect.

Discussion

A rapidly-expanding body of work points to the LPBN as a critical hub for both pain and emotional-motivational processing (for recent review, see Palmiter, 2018; Chiang et al., 2019). Modulation of LPBN activity seems to provide a mechanism for shifting throughout the emotional-motivational continuum, with LPBN excitation/disinhibition exerting pro-aversive and anti-appetitive effects, and LPBN inhibition producing the opposite result (Han et al., 2015; Roman et al., 2016; Douglass et al., 2017; Alhadeff et al., 2018; Chiang et al., 2020; Raver et al., 2020; Sun et al., 2020; Luskin et al., 2021). Here, we focused on the role of GABAergic CeA neurons that express the CaMKIIα gene and project to the LPBN. We report that selective activation of this limbic output is sufficient for reducing neuronal and behavioral responses to painful stimuli, reducing defensive behavior evoked by non-noxious stimuli, and promoting appetitive behavior.

Modulation of nociceptive processing

Inhibition of excitatory LPBN neurons reduces nocifensive and emotional responses to noxious stimuli in rodents (Chiang et al., 2020; Raver et al., 2020; Sun et al., 2020). Here, we show that CeA^{CAM} input similarly inhibited LPBN responses evoked by

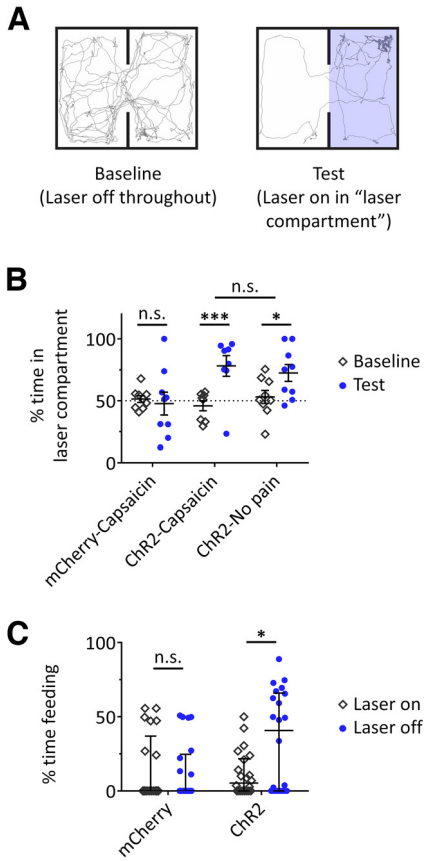

Figure 6. Optogenetic stimulation of CeA^{CAM}-LPBN projections induces place preference and promotes feeding in sated rats. ***A***, Example tracks from one AAV-ChR2 rat in the RTPP paradigm. This rat showed no preference to either side of the 2-compartment arena during the baseline session (left), in which no laser stimulation was given. In contrast, in the test session (right), this rat showed a strong preference to the compartment in which it received laser stimulation (blue shading). ***B***, Summary of RTPP results from all three groups: capsaicin-injected AAV-mCherry rats ($n = 9$); capsaicin-injected AAV-ChR2 rats ($n = 8$); untreated AAV-ChR2 rats ($n = 9$). Both the ChR2-Capsaicin group and the ChR2-No pain group showed a significantly increased preference to the laser compartment in the test session, compared with the baseline session (**$p = 0.0003$ and *$p = 0.018$, respectively). There was no significant difference between both ChR2 groups in the % time spent in the laser chamber during the baseline or test sessions ($p = 0.67$ for both). AAV-mCherry rats showed no increased preference to the laser compartment during the test session ($p > 0.9$). ***C***, Effect of laser stimulation on feeding in sated rats. In the AAV-mCherry group ($n = 21$), the % of time spent feeding was not affected by laser stimulation ($p > 0.99$). In contrast, AAV-ChR2 rats spent significantly more time feeding during laser stimulation periods as compared with laser off periods (*$p = 0.013$). Horizontal lines and error bars show medians and interquartile ranges, respectively. ***B***, ***C***, n.s. = non significant.

putative Aδ- and C-fiber activation in a $GABA_A$ receptor-dependent manner, and was effective in attenuating LPBN responses to mechanical, thermal, and chemical noxious stimuli.

"Nociceptive" LPBN neurons typically exhibited sparse spontaneous firing, and responded selectively to noxious stimuli, in line with previous reports (Bernard and Besson, 1990; Bester et al., 1995; Nakamura and Morrison, 2008). Interestingly, although CeA^{CAM}-LPBN stimulation dampened evoked responses overall, it did not eliminate intensity coding, as indicated by the similar slopes of the stimulus-response curves to mechanical stimuli in the laser off and laser on conditions. Similarly, stimulation of CeA^{CAM}-LPBN projections decreased capsaicin-induced LPBN responses, but did not abolish them. In behaving animals, CeA^{CAM}-LPBN stimulation reduced mechanical and thermal sensitivity; while capsaicin-induced hypersensitivity was also reduced, threshold values during optogenetic stimulation did not reach precapsaicin levels. These results suggest that activation of LPBN $GABA_A$ receptors by CeA^{CAM} neurons interacts with excitatory nociceptive input to shape LPBN output.

CeA^{CAM}-modulated responses were observed in various subregions of the LPBN previously reported to receive nociceptive spinoparabrachial projections (Jasmin et al., 1997; Choi et al., 2020). The projection targets of LPBN neurons reportedly correlate with the location of their somata within LPBN subregions (Han et al., 2015; Rodriguez et al., 2017; Chiang et al., 2020; Sun et al., 2020; Barik et al., 2021), suggesting that CeA^{CAM} input can modulate nociceptive signals conveyed by the LPBN to numerous brain regions involved in various functions. Thus, CeA^{CAM}-LPBN projections seem to be poised to modulate multiple aspects of pain processing. Our behavioral data show that activation of this pathway reduced nocifensive responses to both mechanical and thermal stimulation, and also interfered with the ability of a noxious shock to act as a teaching signal in a threat conditioning paradigm. Notably, CeA^{CAM}-LPBN stimulation during foot-shock did not reduce shock-induced freezing, suggesting that optogenetic stimulation was more effective in suppressing nociceptive LPBN output to areas involved in aversive learning (e.g., CeA) than to areas involved in innate defensive behavior (e.g., PAG; Han et al., 2015; Deng et al., 2016; Yu et al., 2017; Chiang et al., 2020). However, this interpretation should be made with caution, as some rats respond to shocks with increased mobility rather than freezing; this active coping strategy may obscure the observed effect of optogenetic stimulation.

Modulation of emotional-motivation behavior

The current study adds to previous work showing emotional-motivational effects of LPBN activity. Interestingly, LPBN inhibition can affect emotional-motivational behavior even in the absence of nociceptive input (Figs. 5, 6; Douglass et al., 2017). This seem to be at odds with the sparse activity of LPBN neurons in the absence of nociceptive input. A possible explanation is that spontaneous LPBN activity is suppressed under anesthesia, and is substantially higher in awake animals (J. Smith and A. Keller, personal communication). Conceivably, LPBN neurons can be activated by various non-noxious yet aversive/threatening inputs commonly present in experimental settings. For instance, LPBN activity is elevated by the presentation of a tone that was previously paired with a noxious shock (Campos et al., 2018). Exposure within a novel open field may similarly drive thigmotaxis behavior via LPBN activation. Our results indicate that LPBN inhibition can counteract defensive behaviors induced by such non-noxious stimuli.

In addition, we show that CeA^{CAM}-LPBN stimulation was similarly rewarding in the presence and absence of nociceptive input, as tested in the RTPP paradigm. These data further support the notion that the emotional-motivational effects induced by this pathway are not merely the result of reduced nociceptive drive. Rather, it seems that nociceptive and emotional-motivational processing at the LPBN level are at least partially independent. Additional work would be required to systematically address this point.

Role of CeA^{CAM}-LPBN neurons within the amygdalar circuitry

Historically, activation of CeA neurons has been thought to primarily induce fear and aversion (LeDoux and Daw, 2018). Neurons in the lateral-capsular CeA receive excitatory input from LPBN neurons signaling a broad range of aversive stimuli

(Han et al., 2015; Campos et al., 2018; Wilson et al., 2019). CeA-PAG projections control stress-induced analgesia through indirect descending inhibition of spinal neurons, while simultaneously evoking defensive responses (Helmstetter, 1992; Sandkühler, 1996; Butler and Finn, 2009; Tovote et al., 2015; LeDoux and Daw, 2018; Mobbs et al., 2020). However, some CeA neurons seem to serve both anti-nociceptive as well as anti-aversive functions (Hua et al., 2020). Given the effects of LPBN inhibition on pain and aversion, GABAergic CeA-LPBN neurons are likely substrates for this function.

We show that the vast majority of GABAergic LPBN-projecting CeA neurons express CaMKIIα mRNA, in stark contrast to the neocortex, hippocampus, and basolateral amygdalar complex, where CaMKIIα is expressed in glutamatergic cells (Corder et al., 2019; Magnus et al., 2019; S. Kim et al., 2020; An et al., 2021). The fact that CeA^{CAM}-LPBN neurons express the CaMKIIα gene suggests that they are under excitatory control (Incontro et al., 2018), the source of which remains to be elucidated. One likely candidate is the basolateral amygdala, as some of its excitatory projections to the CeA were shown to have both analgesic and appetitive functions (J. Kim et al., 2017; Cai et al., 2018). Given the vital role of CaMKIIα in synaptic plasticity (Malenka and Nicoll, 1999; Sandkühler and Gruber-Schoffnegger, 2012; Sandkühler and Lee, 2013), an intriguing possibility is that long-term potentiation of basolateral-CeA^{CAM} synapses could induce long-lasting analgesic effects through increased inhibition of LPBN neurons, possibly contributing to pain resilience and counteracting the development of psychological comorbidities frequently observed in pain patients (Radat et al., 2013).

The functional implications of activating GABAergic CeA neurons are diverse, and seem to depend both on their genetic identity as well as their downstream targets. We found that ~90% of CeA^{CAM}-LPBN neurons express somatostatin. This result differs from Raver et al. (2020), who reported somatostatin expression in ~30% of CeA-LPBN neurons, based on different retrograde tracing and mRNA labeling techniques. While activation of somatostatin+ CeA neurons produces analgesic effects (Wilson et al., 2019), their role in aversion and defensive behavior seems complex. On the one hand, activation of somatostatin+ CeA neurons has been reported to induce freezing, likely via disinhibition of excitatory PAG neurons (Tovote et al., 2015, 2016; Li, 2019). On the other hand, optogenetic activation of somatostatin+ CeA neurons was recently reported to promote appetitive behavior, but not freezing (J Kim et al., 2017). Our results indicate that activation of LPBN-projecting somatostatin-expressing CeA neurons produces analgesic, anti-aversive, and pro-appetitive behaviors.

Similarly, we observed that roughly one fifth of CeA^{CAM}-LPBN neurons express CRH. CRH+ CeA neurons, particularly those positioned in the lateral CeA, have been suggested to promote aversive learning and flight responses via intra-CeA circuits and projections to the dorsolateral PAG (Fadok et al., 2017; Sanford et al., 2017; Li, 2019). Intriguingly, it was recently reported that optogenetic stimulation of CRH+ CeA-LPBN projections is sufficient for the attenuation of nocifensive responses to mechanical stimulation in naive and formalin-treated rats (Raver et al., 2020). The genetic profile of CeA neurons must therefore be considered in the context of their position within specific neuronal circuits.

Functional implications

Our results indicate that activation of CeA^{CAM}-LPBN projections not only inhibits pain responses, but also induces a behavioral shift toward the positive-appetitive pole of the emotional-motivational continuum. This form of descending pain modulation stands in stark contrast to amygdala- and PAG-mediated stress-induced analgesia, where the inhibition of ascending pain signals is accompanied by aversion and defensive behavior. Conceivably, CeA^{CAM}-LPBN projections would become active when an animal must overcome a noxious or aversive experience to address appetitive motivations such as feeding or copulation; in such scenarios, it would be advantageous to suppress pain without disrupting the appetitive motivational state. Future treatments enhancing CeA^{CAM}-LPBN signaling may hold substantial benefits for pain patients. Hypothetically, such treatments would not only decrease pain sensation, but would also reduce the prevalence of negative coping strategies such as avoidance and catastrophizing, and promote a positive affective state that may support recuperation.

References

Alhadeff AL, Su Z, Hernandez E, Klima ML, Phillips SZ, Holland RA, Guo C, Hantman AW, De Jonghe BC, Betley JN (2018) A neural circuit for the suppression of pain by a competing need state. Cell 173:140–152.

An S, Wang J, Zhang X, Duan Y, Xu Y, Lv J, Wang D, Zhang H, Richter-Levin G, Klavir O, Yu B, Cao X (2021) αCaMKII in the lateral amygdala mediates PTSD-Like behaviors and NMDAR-dependent LTD. Neurobiol Stress 15:100359.

Applegate CD, Kapp BS, Underwood MD, McNall CL (1983) Autonomic and somatomotor effects of amygdala central N. stimulation in awake rabbits. Physiol Behav 31:353–360.

Bardo MT, Bevins RA (2000) Conditioned place preference: what does it add to our preclinical understanding of drug reward? Psychopharmacology (Berl) 153:31–43.

Barik A, Thompson JH, Seltzer M, Ghitani N, Chesler AT (2018) A brainstem-spinal circuit controlling nocifensive behavior. Neuron 100:1491–1503.

Barik A, Sathyamurthy A, Thompson J, Seltzer M, Levine A, Chesler A (2021) A spinoparabrachial circuit defined by Tacr1 expression drives pain. Elife 10:e61135.

Barnett SA (1963) The rat: a study in behavior. Chicago: AldineTransaction.

Bernard JF, Besson JM (1990) The spino(trigemino)pontoamygdaloid pathway: electrophysiological evidence for an involvement in pain processes. J Neurophysiol 63:473–490.

Bester H, Menendez L, Besson JM, Bernard JF (1995) Spino (trigemino) parabrachiohypothalamic pathway: electrophysiological evidence for an involvement in pain processes. J Neurophysiol 73:568–585.

Bonin RP, Bories C, De Koninck Y (2014) A simplified up-down method (SUDO) for measuring mechanical nociception in rodents using von Frey filaments. Mol Pain 10:26.

Butler RK, Finn DP (2009) Stress-induced analgesia. Prog Neurobiol 88:184–202.

Cai YQ, Wang W, Paulucci-Holthauzen A, Pan ZZ (2018) Brain circuits mediating opposing effects on emotion and pain. J Neurosci 38:6340–6349.

Campos CA, Bowen AJ, Roman CW, Palmiter RD (2018) Encoding of danger by parabrachial CGRP neurons. Nature 555:617–622.

Chiang MC, Bowen A, Schier LA, Tupone D, Uddin O, Heinricher MM (2019) Parabrachial complex: a hub for pain and aversion. J Neurosci 39:8225–8230.

Chiang MC, Nguyen EK, Canto-Bustos M, Papale AE, Oswald AM, Ross SE (2020) Divergent neural pathways emanating from the lateral parabrachial nucleus mediate distinct components of the pain response. Neuron 106:927–939.

Choi S, Hachisuka J, Brett MA, Magee AR, Omori Y, Iqbal NU, Zhang D, DeLisle MM, Wolfson RL, Bai L, Santiago C, Gong S, Goulding M, Heintz N, Koerber HR, Ross SE, Ginty DD (2020) Parallel ascending spinal pathways for affective touch and pain. Nature 587:258–263.

Corder G, Ahanonu B, Grewe BF, Wang D, Schnitzer MJ, Scherrer G (2019) An amygdalar neural ensemble that encodes the unpleasantness of pain. Science 363:276–281.

Deng H, Xiao X, Wang Z (2016) Periaqueductal gray neuronal activities underlie different aspects of defensive behaviors. J Neurosci 36:7580–7588.
Douglass AM, Kucukdereli H, Ponserre M, Markovic M, Gründemann J, Strobel C, Alcala Morales PL, Conzelmann KK, Lüthi A, Klein R (2017) Central amygdala circuits modulate food consumption through a positive-valence mechanism. Nat Neurosci 20:1384–1394.
Fadok JP, Krabbe S, Markovic M, Courtin J, Xu C, Massi L, Botta P, Bylund K, Müller C, Kovacevic A, Tovote P, Lüthi A (2017) A competitive inhibitory circuit for selection of active and passive fear responses. Nature 542:96–100.
Fanselow MS, Hoffman AN, Zhuravka I (2019) Timing and the transition between modes in the defensive behavior system. Behav Processes 166:103890.
Gauriau C, Bernard JF (2002) Pain pathways and parabrachial circuits in the rat. Exp Physiol 87:251–258.
Hadschieff V, Drdla-Schutting R, Springer DN, Siegert ASM, Schroeder H, Sandkühler J (2020) Fundamental sex differences in morphine withdrawal-induced neuronal plasticity. Pain 161:2022–2034.
Han S, Soleiman MT, Soden ME, Zweifel LS, Palmiter RD (2015) Elucidating an affective pain circuit that creates a threat memory. Cell 162:363–374.
Hargreaves K, Dubner R, Brown F, Flores C, Joris J (1988) A new and sensitive method for measuring thermal nociception in cutaneous hyperalgesia. Pain 32:77–88.
Helmstetter FJ (1992) The amygdala is essential for the expression of conditional hypoalgesia. Behav Neurosci 106:518–528.
Hua T, Chen B, Lu D, Sakurai K, Zhao S, Han BX, Kim J, Yin L, Chen Y, Lu J, Wang F (2020) General anesthetics activate a potent central pain-suppression circuit in the amygdala. Nat Neurosci 23:854–868.
Incontro S, Díaz-Alonso J, Iafrati J, Vieira M, Asensio CS, Sohal VS, Roche KW, Bender KJ, Nicoll RA (2018) The CaMKII/NMDA receptor complex controls hippocampal synaptic transmission by kinase-dependent and independent mechanisms. Nat Commun 9:2069.
Jasmin L, Burkey AR, Card JP, Basbaum AI (1997) Transneuronal labeling of a nociceptive pathway, the spino-(trigemino-)parabrachio-amygdaloid, in the rat. J Neurosci 17:3751–3765.
Jia HG, Zhang GY, Wan Q (2005) A GABAergic projection from the central nucleus of the amygdala to the parabrachial nucleus: an ultrastructural study of anterograde tracing in combination with post-embedding immunocytochemistry in the rat. Neurosci Lett 382:153–157.
Karoly P, Ruehlman LS (2006) Psychological "resilience" and its correlates in chronic pain: findings from a national community sample. Pain 123:90–97.
Kim J, Zhang X, Muralidhar S, LeBlanc SA, Tonegawa S (2017) Basolateral to central amygdala neural circuits for appetitive behaviors. Neuron 93:1464–1479.
Kim S, Kyung T, Chung JH, Kim N, Keum S, Lee J, Park H, Kim HM, Lee S, Shin HS, Heo WD (2020) Non-invasive optical control of endogenous Ca^{2+} channels in awake mice. Nat Commun 11:210.
Lang PJ, Bradley MM (2010) Emotion and the motivational brain. Biol Psychol 84:437–450.
LeDoux J, Daw ND (2018) Surviving threats: neural circuit and computational implications of a new taxonomy of defensive behaviour. Nat Rev Neurosci 19:269–282.
LeDoux JE, Iwata J, Cicchetti P, Reis DJ (1988) Different projections of the central amygdaloid nucleus mediate autonomic and behavioral correlates of conditioned fear. J Neurosci 8:2517–2529.
Li B (2019) Central amygdala cells for learning and expressing aversive emotional memories. Curr Opin Behav Sci 26:40–45.
Luskin AT, Bhatti DL, Mulvey B, Pedersen CE, Girven KS, Oden-Brunson H, Kimbell K, Blackburn T, Sawyer A, Gereau RW, Dougherty JD, Bruchas MR (2021) Extended amygdala-parabrachial circuits alter threat assessment and regulate feeding. Sci Adv 7:eabd3666.
Magnus CJ, Lee PH, Bonaventura J, Zemla R, Gomez JL, Ramirez MH, Hu X, Galvan A, Basu J, Michaelides M, Sternson SM (2019) Ultrapotent chemogenetics for research and potential clinical applications. Science 364:eaav5282.
Malenka RC, Nicoll RA (1999) Long-term potentiation–a decade of progress? Science 285:1870–1874.
Mobbs D, Headley DB, Ding W, Dayan P (2020) Space, time, and fear: survival computations along defensive circuits. Trends Cogn Sci 24:228–241.
Mody I, Pearce RA (2004) Diversity of inhibitory neurotransmission through GABA(A) receptors. Trends Neurosci 27:569–575.
Nakamura K, Morrison SF (2008) A thermosensory pathway that controls body temperature. Nat Neurosci 11:62–71.
Neugebauer V, Mazzitelli M, Cragg B, Ji G, Navratilova E, Porreca F (2020) Amygdala, neuropeptides, and chronic pain-related affective behaviors. Neuropharmacology 170:108052.
Oliveira MA, Prado WA (2001) Role of PAG in the antinociception evoked from the medial or central amygdala in rats. Brain Res Bull 54:55–63.
Palmiter RD (2018) The parabrachial nucleus: CGRP neurons function as a general alarm. Trends Neurosci 41:280–293.
Paxinos G, Watson C (2007) The rat brain in stereotaxic cooridnates. New York: Academic Press.
Radat F, Margot-Duclot A, Attal N (2013) Psychiatric co-morbidities in patients with chronic peripheral neuropathic pain: a multicentre cohort study. Eur J Pain 17:1547–1557.
Raver C, Uddin O, Ji Y, Li Y, Cramer N, Jenne C, Morales M, Masri R, Keller A (2020) An amygdalo-parabrachial pathway regulates pain perception and chronic pain. J Neurosci 40:3424–3442.
Rhudy JL, Meagher MW (2001) The role of emotion in pain modulation. Curr Opin Psychiatry 14:241–245.
Rodriguez E, Sakurai K, Xu J, Chen Y, Toda K, Zhao S, Han B-X, Ryu D, Yin H, Liedtke W, Wang F (2017) A craniofacial-specific monosynaptic circuit enables heightened affective pain. Nat Neurosci 20:1734–1743.
Roman CW, Derkach VA, Palmiter RD (2016) Genetically and functionally defined NTS to PBN brain circuits mediating anorexia. Nat Commun 7:11905.
Sandkühler J (1996) The organization and function of endogenous antinociceptive systems. Prog Neurobiol 50:49–81.
Sandkühler J, Gruber-Schoffnegger D (2012) Hyperalgesia by synaptic long-term potentiation (LTP): an update. Curr Opin Pharmacol 12:18–27.
Sandkühler J, Lee J (2013) How to erase memory traces of pain and fear. Trends Neurosci 36:343–352.
Sanford CA, Soden ME, Baird MA, Miller SM, Schulkin J, Palmiter RD, Clark M, Zweifel LS (2017) A central amygdala CRF circuit facilitates learning about weak threats. Neuron 93:164–178.
Shrivastava AN, Triller A, Sieghart W (2011) $GABA_A$ receptors: post-synaptic co-localization and cross-talk with other receptors. Front Cell Neurosci 5:7.
Sturgeon JA, Zautra AJ, Arewasikporn A (2014) A multilevel structural equation modeling analysis of vulnerabilities and resilience resources influencing affective adaptation to chronic pain. Pain 155:292–298.
Sullivan GM, Apergis J, Gorman JM, LeDoux JE (2003) Rodent doxapram model of panic: behavioral effects and c-Fos immunoreactivity in the amygdala. Biol Psychiatry 53:863–870.
Sun L, Liu R, Guo F, Wen MQ, Ma XL, Li KY, Sun H, Xu CL, Li YY, Wu MY, Zhu ZG, Li XJ, Yu YQ, Chen Z, Li XY, Duan S (2020) Parabrachial nucleus circuit governs neuropathic pain-like behavior. Nat Commun 11:5974.
Thomson AM, Jovanovic JN (2010) Mechanisms underlying synapse-specific clustering of GABA(A) receptors. Eur J Neurosci 31:2193–2203.
Tovote P, Fadok JP, Lüthi A (2015) Neuronal circuits for fear and anxiety. Nat Rev Neurosci 16:317–331.
Tovote P, Esposito MS, Botta P, Chaudun F, Fadok JP, Markovic M, Wolff SB, Ramakrishnan C, Fenno L, Deisseroth K, Herry C, Arber S, Lüthi A (2016) Midbrain circuits for defensive behaviour. Nature 534:206–212.
Uddin O, Studlack P, Akintola T, Raver C, Castro A, Masri R, Keller A (2018) Amplified parabrachial nucleus activity in a rat model of trigeminal neuropathic pain. Neurobiol Pain 3:22–30.
Wilson TD, Valdivia S, Khan A, Ahn HS, Adke AP, Martinez GS, Sugimura YK, Carrasquillo Y (2019) Dual and opposing functions of the central amygdala in the modulation of pain. Cell Rep 29:332–346.
Xanthos DN, Gaderer S, Drdla R, Nuro E, Abramova A, Ellmeier W, Sandkühler J (2011) Central nervous system mast cells in peripheral inflammatory nociception. Mol Pain 7:42–58.
Yu K, Ahrens S, Zhang X, Schiff H, Ramakrishnan C, Fenno L, Deisseroth K, Zhao F, Luo M-H, Gong L, He M, Zhou P, Paninski L, Li B (2017) The central amygdala controls learning in the lateral amygdala. Nat Neurosci 20:1680–1685.